Wireless Channel Characterization: Modeling the 5 GHz Microwave Landing System Extension Band for Future Airport Surface Communications[1]

D. W. Matolak, I. Sen, W. Xiong
School of EECS
Avionics Engineering Center
Ohio University
Athens, OH 45701
phone: 740.593.1241
fax: 740.593.0007
matolak@ohiou.edu

R. Apaza
Federal Aviation Admin.
Aviation Research Office
Belleville, MI
phone: 734.955.5190
fax: 734.955.5273
rafael.Apaza@faa.gov

L. Foore
NASA Glenn Research Center
Cleveland, OH 44135
phone: 216.433.2346
fax: 216.433.3478
Lawrence.R.Foore@grc.nasa.gov

***Abstract*--We describe a recently completed wideband wireless channel characterization project for the 5 GHz Microwave Landing System (MLS) "extension" band, for airport surface areas. This work included mobile measurements at large and small airports, and fixed point-to-point measurements. Mobile measurements were made via transmission from the air traffic control tower (ATCT), or from an airport "field site" (AFS), to a receiving ground vehicle on the airport surface. The point-to-point measurements were between ATCT and AFSs. Detailed statistical channel models were developed from all these measurements. Measured quantities include propagation path loss and power delay profiles, from which we obtain delay spreads, frequency domain correlation (coherence bandwidths), fading amplitude statistics, and channel parameter correlations. In this paper we review the project motivation, measurement coordination, and illustrate measurement results. Example channel modeling results for several propagation conditions are also provided, highlighting new findings.**

I. INTRODUCTION

The need for new wireless communication services on the airport surface area is well known [1]. Growth in airport operations is expected to continue, and along with this growth will come greater demands for reliable communication services for multiple applications [2]. Given the spectral "congestion" in the aeronautical VHF band [3], the aviation community has naturally turned toward other aviation frequency bands to assess the ability of these bands to meet future needs. The Microwave Landing System (MLS) extension band, from 5.091-5.15 GHz, represents one such band.

The MLS extension band is not widely used, and because of this, offers ample spectrum in which to deploy communication systems for the airport surface environment. Noteworthy is that because of the sparse usage of this band, other (non-aviation) organizations view this spectrum as not needed by the aviation community. Hence, these organizations are likely to propose that this spectrum's allocation be changed to *non*-aviation usage. The aviation community's response to this has been to organize delegations, through the International Civil Aviation Organization (ICAO), to the International Telecommunications Union's (ITU's) World Radio Conference, to illustrate the aviation community's need for, and imminent use of, this band.

Measurement of the channel characteristics of this band around airport surface areas represents the first step in a systematic engineering process that will culminate with deployed airport surface communication networks. In a prior paper [4], we described this motivation, example uses of detailed channel models, and some example measurement results. In this paper, we conclude the project with a review of its key aspects, which includes the multiple motivations for the work, required

[1] This work was supported by NASA Glenn Research Center, under award number NNC04GB45G.

coordination activities for successful measurements, and the measurement and modeling outputs.

Section II briefly describes the regulatory issues motivating this work. Section III describes the measurement coordination activities at the multiple airports measured. In Section IV, we review the measurement procedures and outputs, and provide example measured results. Section V describes modeling results and Section VI concludes the paper with a summary and recommendations.

II. REGULATORY ISSUES

As noted, the MLS extension band is of great current interest to the aeronautical community. The lead organization is ICAO, who is working to ensure that this spectral band remains allocated for aeronautical services, by ensuring aviation community delegations participate in the next World Radio Conference (WRC) of the ITU in 2007. The United States Federal Aviation Administration, and the European Union's aviation administration, EuroControl, are supporting ICAO in this effort.

At the next WRC, member nations will discuss and decide upon the global use of radio spectrum for multiple applications. Aviation related spectrum issues exist for frequency bands from 108 MHz to 6 GHz. One of the intentions of the ACAST project was to demonstrate the suitability of the MLS extension band for wideband airport surface area signaling. One reason for this is the possible "relief" this could provide by "offloading" some of the congested VHF voice bands used by pilots and air traffic controllers.

Since the MLS extension band is just below a 5 GHz WLAN band in frequency, it represents an attractive way for WLAN manufacturers and system developers to gain system capacity. Thus, real "threats" to the exclusive aviation use of this band exist. In addition, GPS navigation and WAAS/LAAS enhancements appear to be circumventing the need for new MLS deployments. This has left most of this band underutilized. Both these factors have motivated the aviation community's need to justify the continued exclusive use of this spectrum for aviation purposes.

In addition, the growth of air travel and airport services will only increase the need for new reliable communication systems. The band thus can contribute to the Next Generation Air Transportation System's modernization effort. In addition, the channel characterization effort can be viewed as one of the first substantive activities that illustrate the seriousness of the aviation community in using this band.

Some of the preliminary channel characterization results have been input to ICAO as working documents toward use of this band. In the future, the final channel characterization outputs will be made fully available to this organization, to support future aeronautical use of this important spectral band.

III. MEASUREMENT COORDINATION

The coordination required to conduct measurement activities at an airport facility is not trivial. To characterize the MLS band in an airport environment, access to airport facility information, airport facilities themselves (physical access), and to the protected spectral band (medium access) is required. Successfully achieving access to these different coordination components required careful planning to execute a non-disruptive measurement campaign. Additionally, close collaboration with FAA Airways Facilities personnel, FAA Air Traffic Control, and measurement team members was necessary to maximize efficiency, and minimize impacts to airport operations.

Access to airport information is a key requirement, which enabled the development of a measurement strategy, establishment of procedures, equipment deployment planning, and a coordinated team approach. The Air Traffic Control Tower information aided in identifying the optimal deployment of the sounder transmitter system, power source, sounder system synchronization location and more. Airport layout information obtained from the FAA enabled selection of ideal measurement locations, preliminary parameter estimation, and measurement route determination. Figure 1 shows measurement locations identified for John

F. Kennedy International Airport, in New York, NY. Using this type of information enabled FAA Airways Facilities, Air Traffic personnel, and the measurement team to optimize measurement locations and procedures.

Physical access to airport facilities has always been difficult and, in the post 9/11era, it has grown in difficulty and complexity. To gain access to airport grounds, personnel and vehicular requirements needed to be addressed. Before an individual is authorized access to airport facilities, a background check is conducted. Foreign nationals are required to provide passport and other necessary documentation to complete a security clearance. Access to restricted areas required proper badge and identification for all individuals conducting measurements. Once on airport grounds or facilities, non-FAA team members required the presence of an FAA escort at all times. Access for vehicles not authorized to operate on airport grounds was coordinated with FAA and airport security. Ideally, access to airport movement areas was desired at times of high aircraft activity to obtain maximum traffic effects upon channel characteristics (e.g., signal reflections). This was achieved with assistance from Air Traffic Control and Airway Facilities personnel who drove to all measurement locations with the measurement team.

Coordinating access to the transmission medium required participation by government agencies other than NASA and FAA. The MLS band is internationally allocated to Aeronautical Radio Navigation Service (ARNS). Authorization to radiate in this band required two coordinated activities. First, the FAA spectrum engineering office conducted a Radio Frequency Interference (RFI) analysis for each airport facility that was measured. To conduct this evaluation, information that included transmitter location, power output, antenna characteristics, operating frequency, and other parameters was provided. Second, NASA Glenn Research Center submitted a request for a Special Temporary Authorization (STA) to the National Telecommunications and Information Administration (NTIA). This request included measurement equipment technical information, test duration and locations. The NTIA contacted government offices that could be affected by this measurement activity and requested an evaluation from each agency. Once both activities were successfully completed, a letter indicating the results of both frequency analysis requests was issued to local FAA Airport management and Systems Management Office for review and comments. For all airports at which measurements were done, these activities and authorizations were successfully completed.

In addition to the coordination of physical, medium, and information access, subtle variations existed among airports, which required additional coordination. Working with dedicated and knowledgeable local airport authorities, careful management of time and resources enabled timely completion of the measurement campaigns. A “post analysis” of events following every measurement run resulted in optimization and modification of procedures. In the end, careful attention to detail (by all involved) enabled the achievement of nearly all goals set by the team in a safe and un-intrusive manner.

IV. MEASUREMENTS

The measurement procedure consists of transmission of a test signal from either the ATCT or an AFS, and receiving and storing the signal samples obtained with a mobile van that traveled through the airport surface areas. We used the popular direct-sequence spread spectrum (DS-SS) correlator signaling approach [5], with a bandwidth of 50 MHz, and transmit power of 2 W. The transmitter receiver pair, denoted the “sounder,” is a customized version of those used for other bands [6]. Figure 2 shows a photograph of the sounder transmitter (Tx) platform on the Miami Airport ATCT catwalk.

The primary characteristics measured are power delay profiles (PDPs), which estimate the channel impulse response (CIR). The PDPs were taken for various segments of travel over the airport surface, which covered runways, taxiways, cargo areas, access roads, and near airport gates. Both line of sight (LOS) and non-LOS (NLOS) regions were covered, with the majority of the data taken in the NLOS regions, as these pose the greater challenge for reliable communications.

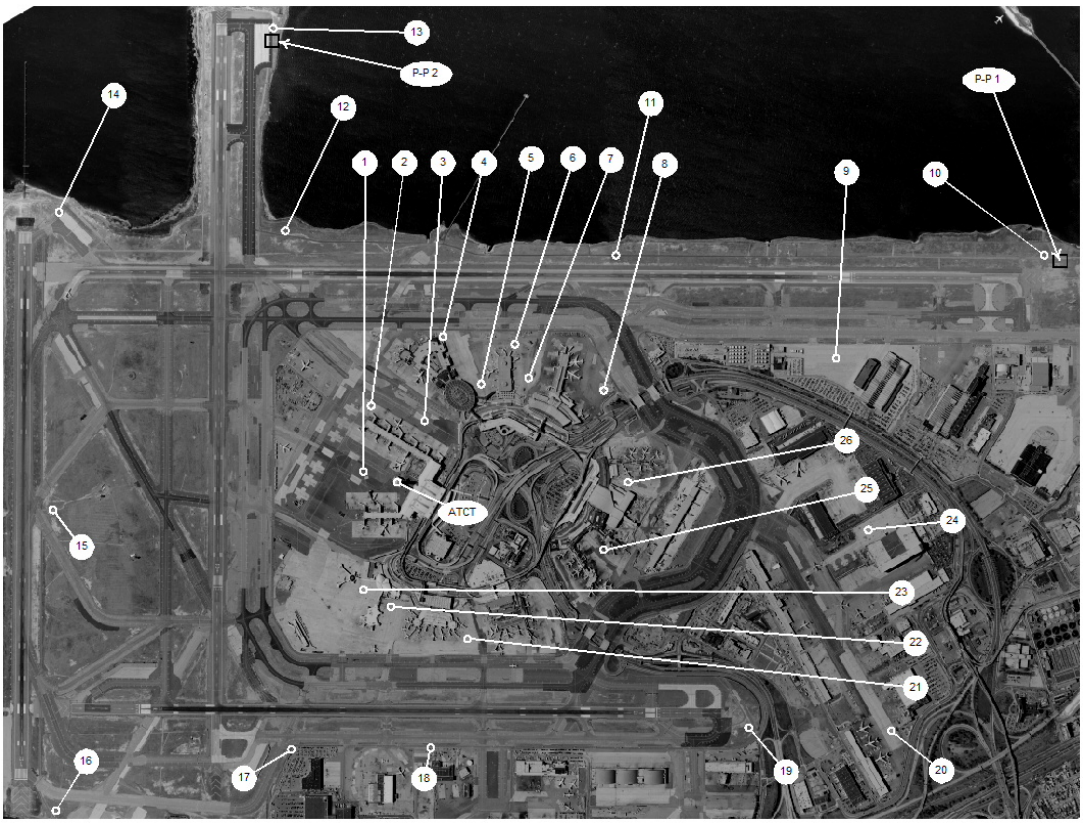

Fig. 1. Aerial photograph of JFK International airport, showing numbered measurement locations.

As is widely done for other applications, our CIRs are characterized statistically [7]. One of the most important CIR statistics is their root-mean-square (RMS) value of delay spread (RMS-DS). This statistic measures the spread of the signal in time, and its frequency domain counterpart, the frequency correlation estimate (FCE, analogous to coherence bandwidth), captures the selectivity of the channel in frequency. We also model the time variation of the amplitudes (fading) statistically.

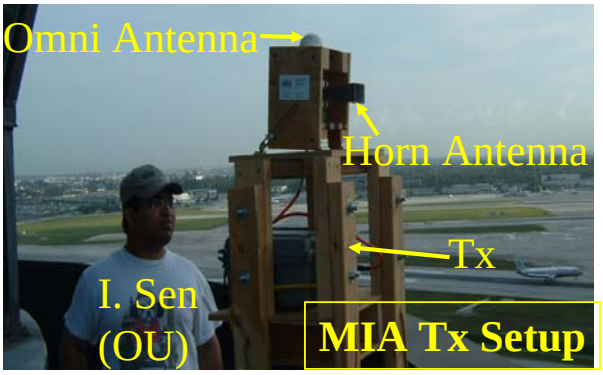

Fig. 2. Photo of sounder Tx at MIA.

Channels were measured at six airports, two large airports (Miami and JFK), one medium airport (Cleveland), and three GA airports (Ohio University, Burke Lakefront, and Tamiami). In addition, we classified the airport surface area into three distinct propagation regions: LOS-Open (LOS-O), NLOS-Specular (NLOS-S), and NLOS, from least to most dispersive, respectively. This provides a more precise description than that in [8], for example. Table 1 summarizes the RMS-DS results for all the airports. In total, over 51,000 PDPs were recorded, approximately 35,000 for the mobile setting (Tx at ATCT), 5,000 for the point-to-point setting, and 11,800 mobile PDPs for airport field sites.

Figure 3 shows an example PDP taken for the NLOS region in Miami. The RMS-DS for this profile is approximately 1.43 microseconds; multiple, large amplitude multipath components are visible in addition to the first-arriving component.

Throughout the course of travel on the airport surface, we observed multipath delay

Table 1. Summary RMS-DS measurement results for six airports, three settings.

Measured RMS-DS [min; mean; max] (nanoseconds), Three Settings						
Airport	**Mobile**			**Point-Point**	**Field Site Transmit**	
	NLOS	**NLOS-S**	**LOS-O**	**LOS-O**	**NLOS**	**NLOS-S**
JFK	[800; 1,469; 2,456]	[21.4; 311; 798.7]	—	—	[802; 1,475; 2,433]	[5.8; 317.3; 799.5]
MIA	[1,000; 1,513; 2,415]	[23.1; 459; 999.9]	—	[5.6; 163; 249]	[1,000; 1,625; 2,451]	[8; 443; 997]
CLE	[500; 1,206; 2,472]	[125; 295; 499]	[14; 65; 124]	[1; 18.12; 202]	—	— —
OU	—	[14; 293; 2,416]	—	—	—	— —
BL	—	[126; 429; 2,427]	[5; 44; 124]	—	—	— —
TA	[502; 1,390; 2,404]	[15; 256; 499]	—	—	—	— —

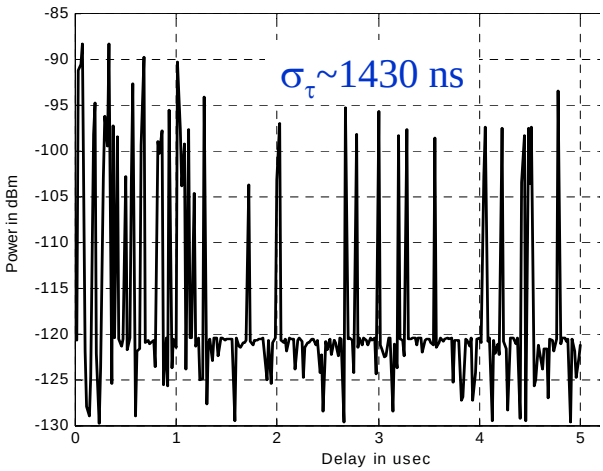

Fig. 3. Example NLOS PDP, MIA.

spreads that changed in time according to the propagation region. This was also manifested in the appearance and disappearance of multipath components. This finite "lifetime" of multipath components we term the "persistence process," and as discussed in the next section, we have developed models for this as well.

Figure 4 shows an example plot of the probability of each multipath component versus delay, for the Miami airport. These are the "steady state" probabilities of the component being present, and are directly used in our persistence process modeling. Example state and transition probability matrices for two of the taps are also provided on this figure.

Figure 5 shows example FCEs, computed according to the method in [9], which does not rely on the traditional wide-sense stationary, uncorrelated scattering (WSSUS) assumption. We found the US assumption often did not hold, implying correlated multipath components. The two FCEs pertain to transmission from the ATCT and from an AFS, computed over the same area of the airport. The wider AFS FCE indicates a less dispersive channel when transmission is from an AFS, supporting their use in future networks.

Figure 6 shows an example time evolution of PDPs in a point-to-point setting, using directional antennas, in Miami. This plot shows PDPs vs. delay and time for the case when the receive antenna is aimed *away* from boresight by approximately 105° in azimuth. The presence of large, stable multipath components, attributable to nearby large buildings, is evident.

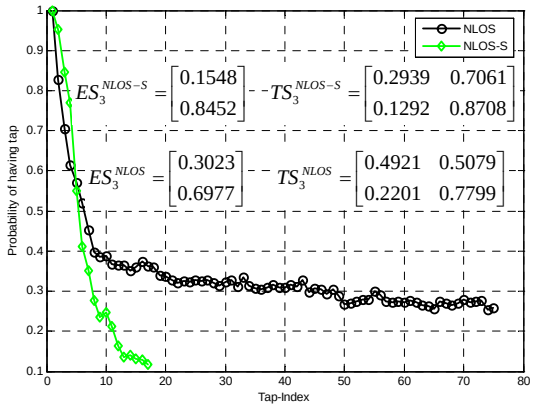

Fig. 4. Example tap probability of occurrence, MIA.

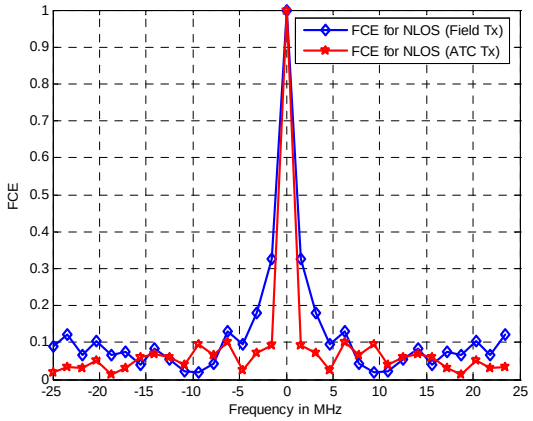

Fig. 5. Example FCEs for NLOS regions in MIA, for both ATCT and AFS transmission.

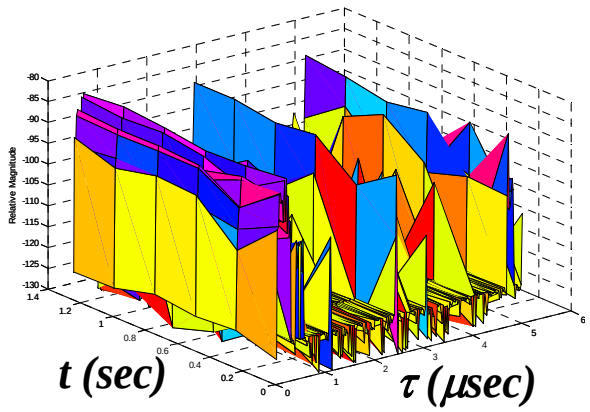

Fig. 6. PDP vs. delay and time, point to point setting, 105° off boresight, MIA.

V. MODELING RESULTS

A. Mobile Channel, Tx at ATCT

As covered in [4] and elsewhere, e.g., [7], [10], the channel models developed are usable by anyone involved in designing or evaluating potential wireless networks for mobile or fixed applications in this setting. To ensure that they are most useful, we adopt the common tapped-delay line model for the channel [11], illustrated in Figure 7. In Figure 7, the *x*'s denote input symbols and the *y*'s output symbols. The τ's are delays, and the *h*'s are the CIR random amplitudes, given by

$$h_k(t) = z_k(t)\alpha_k(t)e^{j\phi_k(t)} \qquad (1)$$

where *k* denotes the channel tap (~multipath component) index, the *z*'s are the tap persistence processes, with $z_k(t) \in \{0,1\}$, the α's are the randomly fading amplitudes, and the ϕ's are the random phases. The number of taps *L* depends on the propagation region (LOS-O, NLOS-S, or NLOS), on the bandwidth of the channel model, and upon the fidelity of the model's representation of the actual channel. The persistence processes and fading amplitudes are modeled as random, with distributions derived empirically. For our "sufficient fidelity" (SF) model, we assume the taps emanate from their estimated distributions, and generate fading samples via appropriate random number generation. We also have a "high fidelity" (HF) model, which uses our actual (stored) data to generate channel samples. In the context of the cellular (COST) models, the SF model is a "synthetic" channel model, and the HF model is a "stored" channel model. For brevity, here we restrict discussion to the SF models only.

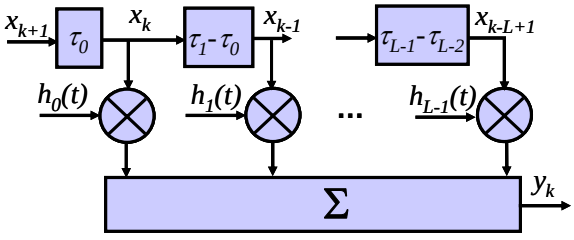

Fig. 7. Tapped delay line channel model.

For illustration, we describe the NLOS region model for the large airport surface environment, for a channel bandwidth (BW) of 10 MHz. From our 50 MHz measurement results, we can construct models for smaller bandwidths easily (and have done so for bandwidths of 20, 10, 5, and 1 MHz). To illustrate the region transitions, we also discuss some parameters of the NLOS-S region for this bandwidth and airport size.

We base the number of channel taps on the mean value of RMS-DS, and for this setting and bandwidth, we obtain values of L_{NLOS}=17 taps, and $L_{NLOS\text{-}S}$=6. We obtain tap steady state probabilities from the empirical data, and the plots for these cases would appear very similar to that shown in Figure 4 for the 50 MHz case, except of course with fewer taps. For the 10 MHz case, the longest-delay ("least persisting") tap has steady state probability greater than 0.65 for the NLOS case, and greater than 0.33 for the NLOS-S case. Given that often, many of the higher-indexed taps—representing longer-delay multipath components—are very low in amplitude in comparison to the lower-indexed taps, we truncate the channel models to contain fewer taps, by considering the cumulative energy in the taps. Relative to a unity total energy, Figure 8 shows cumulative energy vs. tap index for these cases. Based upon Fig. 8, we truncate to L_{NLOS}=14, and $L_{NLOS\text{-}S}$=4 taps, which accounts for approximately 95% and 99% of the total CIR energy, respectively.

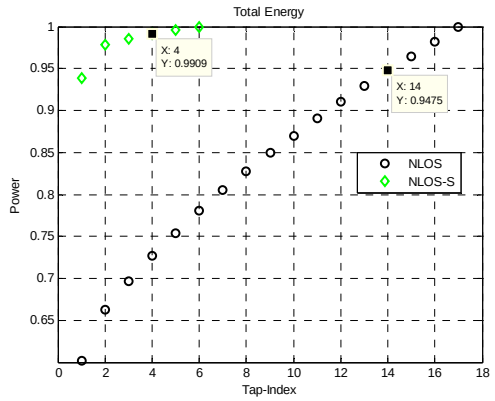

Fig. 8. Cumulative tap energy vs. tap index, large airport, 10 MHz BW, NLOS & NLOS-S regions.

Table 2. NLOS Markov chain tap persistence parameters, 10 MHz.

Tap Index	Steady State Probability P_1	Transition Probability P_{00}	Transition Probability P_{11}
1	1.0000	na	1.0000
2	0.8794	0.1975	0.8899
3	0.7890	0.3258	0.8197
4	0.7747	0.3301	0.8051
5	0.7519	0.3363	0.7809
6	0.7437	0.3599	0.7794
7	0.7288	0.3789	0.7690
8	0.7102	0.4013	0.7556
9	0.7060	0.4063	0.7529
10	0.6930	0.4324	0.7488
11	0.7065	0.4052	0.7528
12	0.7000	0.3868	0.7374
13	0.6798	0.4453	0.7386
14	0.6992	0.4067	0.7449

Table 2 lists persistence process parameters for the NLOS case. For all persistence processes, we use the well-known Markov chain model. The steady state probability for state zero, P_0, is equal to $1\text{-}P_1$, with P_1 the steady state probability for state one. State zero denotes the tap is "off" (below threshold); state one denotes the tap is "on" (above threshold). Similarly, transition probabilities $P_{01}=1\text{-}P_{00}$; $P_{10}=1\text{-}P_{11}$, where P_{ij}=probability of transitioning from state i to j. Figure 9 shows an example time series for the fifth tap in this model, showing the "on/off" switching behavior, for twenty time samples.

For the tap amplitudes, a similar table can be developed; this is shown in Table 3. We have found the Weibull distribution [12] to provide a flexible distribution for fitting all the tap amplitudes. The probability density function for this distribution is given by the following:

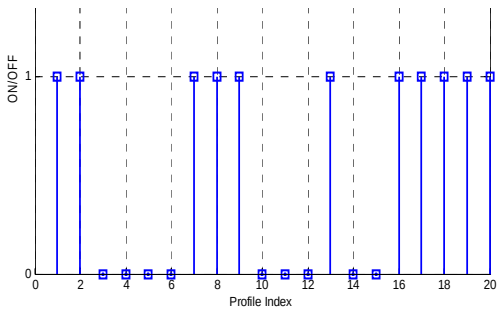

Fig. 9. Example tap persistence time series; tap 5, NLOS, 10 MHz.

$$f_w(x) = \frac{b}{a^b} x^{b-1} \exp\left[-\left(\frac{x}{a}\right)^b\right] \qquad (2)$$

where b is a shape factor that determines fading severity (the smaller the value of b, the worse the fading), and $a=\sqrt{\Omega/\Gamma[(2/b)+1]}$ is a scale parameter, with Ω the mean-square value of the distribution (tap energy), and Γ the Gamma function. A value of b=2 yields the well-known Rayleigh distribution, often used as a near worst-case condition. Note that all but the first tap in Table 3 is "worse than Rayleigh," indicating *severe amplitude fading*. This level of fading has been reported in the literature, for multiple environments, including HF, cellular, and indoor settings, but it is always rare. Also included in Table 3 is the value of the "*m*-parameter" of the Nakagami-*m* distribution.

Figure 10 shows example fits to the distribution for the second tap, for both Weibull and Nakagami-*m*. Good agreement is observed. All fits were maximum likelihood fits.

Once the number of taps, their fading amplitude distributions, and their persistence process parameters are defined, the channel model is nearly complete for the given region. The final step in building the SF model requires that we generate the fading tap amplitude samples in such a way that the tap crosscorrelations accurately reflect the measured data. Simply, each tap amplitude is correlated

Table 3. NLOS fading amp. parameters, 10 MHz.

Tap Index	Weibull Shape Factor (*b*)	Tap Energy	Alternative Distribution Parameter (Nakagami)
1	2.1	0.5273	m = 1.2
2	1.58	0.0605	m = 0.72
3	1.56	0.0382	m = 0.72
4	1.61	0.0346	m = 0.74
5	1.63	0.0315	m = 0.76
6	1.57	0.0310	m = 0.73
7	1.6	0.0302	m = 0.74
8	1.67	0.0276	m = 0.79
9	1.66	0.0266	m = 0.78
10	1.68	0.0248	m = 0.8
11	1.65	0.0262	m = 0.77
12	1.66	0.0260	m = 0.78
13	1.75	0.0234	m = 0.84
14	1.72	0.0230	m = 0.83

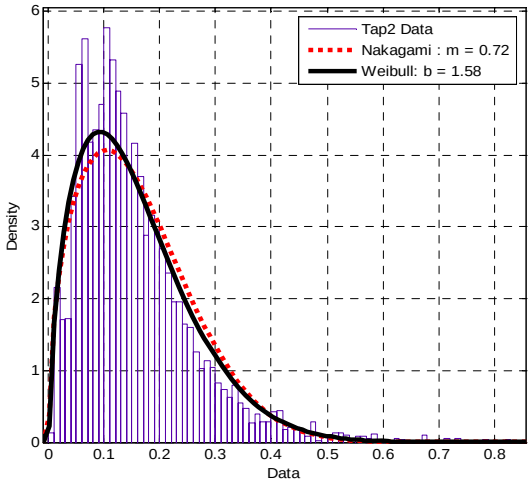

Fig. 10. Example fit to fading amplitude data for NLOS, 10 MHz, second tap.

with all other taps, and this correlation is quantified by the correlation coefficient, which for taps i and j, is given by

$$\rho_{ij} = \frac{Cov(\alpha_i, \alpha_j)}{\sqrt{Var(\alpha_i)Var(\alpha_j)}} \qquad (3)$$

where *Cov* denotes covariance, *Var* denotes variance. Correlated taps represent another atypical finding from our work, as most models assume uncorrelated scattering. The upper left quarter of the correlation matrix $R=[\rho_{ij}]$ is shown in Table 4. Note that some of the taps are highly correlated, e.g., $\rho_{57}\cong 0.7$, for example.

With the tap correlation matrix, all that remains is to generate the random fading amplitude processes and persistence process with the specified parameters, and to allow for switching between propagation regions. For the region switching model, we again use a Markov chain, and for the two regions we model in this example (NLOS and NLOS-S), the Markov transition (*TS*) and steady-state probability (*ES*)

Table 4. Upper right ¼ of NLOS tap correlation matrix, 10 MHz.

	j						
i	**1**	**2**	**3**	**4**	**5**	**6**	**7**
1	1.00	0.592	0.681	0.575	0.644	0.650	0.876
2	0.592	1.00	0.418	0.376	0.549	0.421	0.479
3	0.681	0.418	1.00	0.566	0.758	0.559	0.459
4	0.575	0.376	0.566	1.00	0.998	0.827	0.593
5	0.644	0.549	0.758	0.998	1.00	0.932	0.717
6	0.650	0.421	0.559	0.827	0.932	1.00	0.766
7	0.876	0.479	0.459	0.593	0.717	0.766	1.00

matrices are given in eq. (4), where the propagation states are *2*=NLOS-S and *3*=NLOS.

$$TS = \begin{bmatrix} 0.8840 & 0.1160 \\ 0.1094 & 0.8906 \end{bmatrix} = \begin{bmatrix} P_{22} & P_{23} \\ P_{32} & P_{33} \end{bmatrix}$$

$$ES = \begin{bmatrix} 0.4858 \\ 0.5142 \end{bmatrix} = \begin{bmatrix} P_2 \\ P_3 \end{bmatrix} \quad (4)$$

Figure 11 illustrates conceptually the modeling process used. The equations and tables referred to in this figure pertain to [13].

B. Mobile Channel, Tx at AFS

Similar to modeling for the case with the Tx at the ATCT, results for the mobile channel with the Tx at an AFS can be used to construct models. The exact same procedure can be followed, and will generally yield a channel model with fewer taps, and a larger probability of being in the NLOS-S region than for the Tx at the ATCT.

Due to space limitations we do not show these results here, other than to note that the AFS channel is generally less dispersive than the corresponding ATCT channel. This is illustrated via Figure 12, which shows the distribution of RMS-DS for the two transmission cases, for the exact same portion of the airport surface area, from MIA. The RMS-DS values for the AFS transmission case are generally smaller than those for the ATCT case.

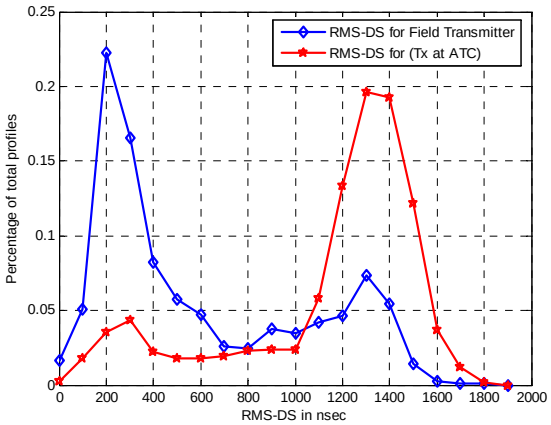

Fig. 12. RMS-DS distribution for section of airport surface in MIA, two Tx locations: ATCT & AFS.

C. Fixed Point-to-Point Channel

For this setting, directional antennas were used at both the ATCT and AFS, and PDP measurements were taken as a function of azimuth angle, as the receive antenna was rotated. For all "boresight" cases, where the antennas were aimed at each other, the channel can be well modeled as having a single tap, with Ricean statistics. For this, the Ricean *K*-factor was typically greater than 20 dB. Figure 13 shows a plot of RMS-DS vs. azimuth angle, from MIA, taken from two AFS locations. In this figure, as well as in the measured PDPs, significant stable reflections from large buildings caused substantial multipath for non-boresight angles. This observation could be useful in AFS siting and in angle diversity

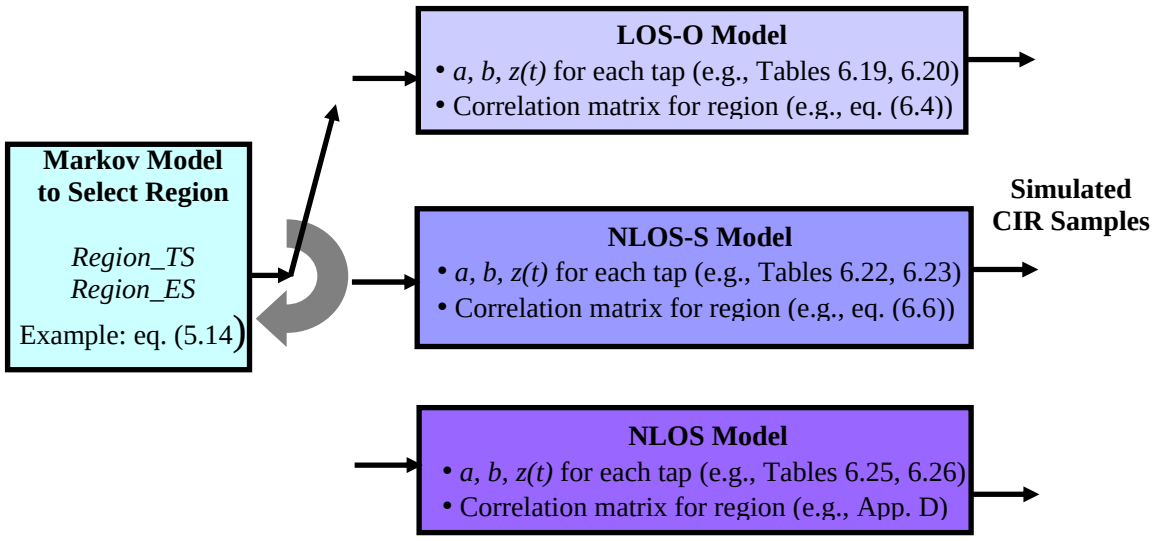

Fig. 11. Conceptual model illustrating generation of non-stationary fading channel samples.

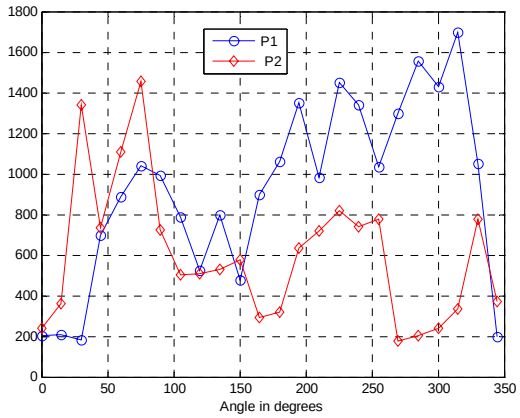

Fig. 13. RMS-DS vs. az. angle, two MIA field sites.

VI. SUMMARY

In this paper, we reviewed work on our completed channel characterization project for the MLS extension band around airport surface areas. We summarized regulatory concerns regarding band use, and also described measurement coordination activities required to successfully complete this project. Measurements were made at airports of three sizes: large, medium, and small (GA).

Example channel measurement results were shown to illustrate some of our findings. One of the most important of these findings is that the airport surface channel is a very dispersive channel (for all but the narrowest of bandwidths, e.g., less than about 1 MHz). The airport surface area can be classified into three propagation regions, with distinct channel characteristics in each. In terms of this dispersion, the NLOS regions have the largest values of RMS delay spread, with large airports having mean spreads of roughly 1.5 microseconds; spreads of approximately 2.2 microseconds represent 99th percentile values. Both severe fading and correlated scattering were observed in the models, both of which are atypical, and create a more challenging channel for reliable communications. We also note that by deploying transmitters at selected airport field sites, signal strength can be improved, and dispersion reduced for areas that are distant and NLOS from the ATCT.

Detailed channel models for the mobile (and non-mobile point-to-point) settings have been developed. These are described in [13].

REFERENCES

[1] NASA ACAST project website, http://acast.grc.nasa.gov/ , 11 April 2006.

[2] Joint Program Development Office (JPDO) website, http://www.jpdo.aero , 11 April 2006.

[3] J. Prinz, et. al., "VHF Channel Occupancy Measurements over Core Europe," *Proc. 5th NASA Integrated Communications, Navigation and Surveillance (ICNS) Conf. & Workshop*, Fairfax, VA, 2-5 May 2005.

[4] D. W. Matolak, L. Foore, R. Apaza, "Channel Characterization in the 5 GHz MLS Extension Band for Future Airport Surface Communications," *Proc. 5th NASA ICNS Conf.*, Fairfax, VA, 2-5 May 2005.

[5] J. D. Parsons, *The Mobile Radio Propagation Channel*, 2nd ed., John Wiley & Sons, New York, NY, 2000.

[6] Berkeley Varitronics, Inc., website, http://www.bvsystems.com/ , 11April 2006.

[7] G. Stuber, *Principles of Mobile Communications*, 2nd ed., Kluwer Academic Publishers, Norwell, MA, 2001.

[8] E. Haas, "Aeronautical Channel Modeling," *IEEE Trans. Vehicular Tech.*, vol. 51, no. 2, pp. 254-264, March 2002.

[9] R. J. C. Bultitude, "Estimating Frequency Correlation Functions from Propagation Measurements on Fading Channels: A Critical Review," *IEEE JSAC*, vol. 20, no. 6, pp. 1133-1143, August 2002.

[10] A. F. Molisch (editor), *Wideband Wireless Digital Communications*, Prentice-Hall, Upper Saddle River, NJ, 2001.

[11] J. G. Proakis, *Digital Communications*, 2nd ed., McGraw-Hill, New York, NY, 1989.

[12] A. Papoulis, A. U. Pillai, *Probability, Random Variables, and Stochastic Processes*, 4th ed., McGraw-Hill, Boston, MA, 2002.

[13] D. W. Matolak, "Wireless Channel Characterization in the 5 GHz Microwave Landing System Extension Band for Airport Surface Areas," NASA ACAST Final Project Report, Grant # NNC04GB45G, April 2006.

OHIO UNIVERSITY

School of Electrical Engineering & Computer Science

Wireless Channel Characterization: Modeling the 5 GHz Microwave Landing System Extension Band for Future Airport Surface Communications*

ICNS Conference, 2 May 2006

D. W. Matolak, I. Sen, W. Xiong
School of EECS, Avionics Eng. Center
Ohio University
Athens, OH 45701
phone: 740.593.1241
fax: 740.593.0007
email: matolak@ohiou.edu

R. Apaza
Federal Aviation Admin.
Aviation Research Office
Belleville, MI
phone: 734.955.5190
fax: 734.955.5273
email:rafael.Apaza@faa.gov

L. Foore
NASA Glenn Research Center
Cleveland, OH 44135
phone: 216.433.2346
fax: 216.433.3478
email:
Lawrence.R.Foore@grc.nasa.gov

**This material is based upon work supported by NASA under grant number NNC04GB45G*

Outline

- Introduction
- Measurement coordination
- Channel characterization & modeling
  - Overview
  - Mobile channel measurements
    - Tx @ ATCT, Rx in Mobile Van
    - Tx @ Ground Site, Rx in Mobile Van
  - Channel model construction
- Summary and future work

Introduction

- Commercial aviation is growing
- In 2003, Congress & Executive Office formed the Joint Planning and Development Office (JPDO) for the Next Generation Air Transportation System (NGATS)
  - DoT, DHS, DoD, DoC, NASA, FAA
  - Now also more than 66 industry & private sector members

Introduction (2): NASA ACAST

- Motivation for work: in line with JPDO…civilian aviation has both near & long-term needs for new communications capabilities
  - VHF spectral "congestion" (118-137 MHz used for analog voice, very low-rate data (2.4 kbps))
  - New services desired, for mobile and "fixed" links, all "phases of flight"
    - En route
    - Takeoff/Landing
    - Taxiing and Parking

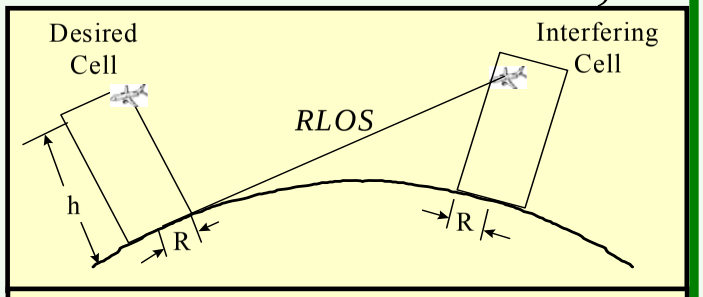

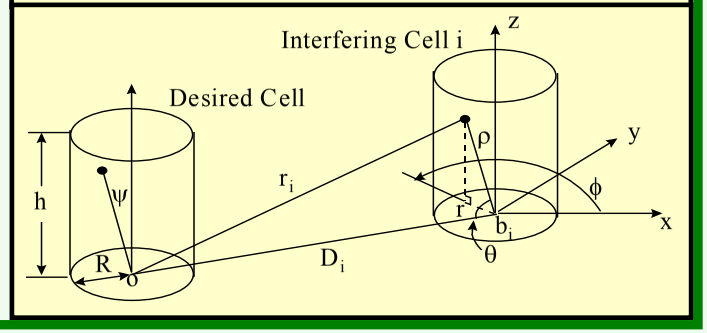

Introduction (3)

- Motivation (cont'd): frequency band selection
  - Easiest to quickly deploy system in "clean" spectrum
  - Deployment of new systems can "protect" reserved aeronautical spectrum ("use it or lose it")
    - International Civil Aviation Organization (ICAO) has delegation for International Telecommunications Union (ITU) World Radio Conference (WRC), next in 2007
  - Microwave landing system (MLS) extension band, 5.091-5.15 GHz, not widely used in many regions meets both the above criteria

OU Airport

Introduction (4)

- Why is channel characterization important?
  - If you don't know your channel, system performance will be suboptimal, possibly very poor, with
    - irreducible channel error rate that can preclude reliable message transfer (ISI)
    - spatial coverage "holes" where communication not possible (shadowing, fading)
    - severely limited data carrying capacity (ISI, fading)

    …all of which could require costly system additions to circumvent
  - Dearth of work for MLS band channel
    - Zero wideband experimental work for this band around airport surfaces

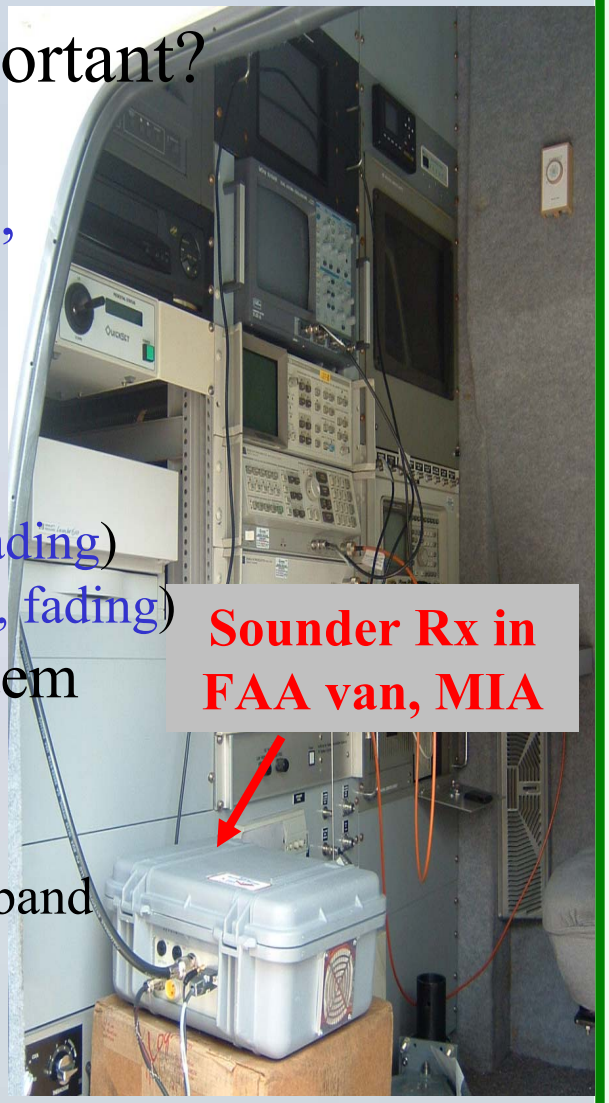

Measurement Coordination

- Measured at three major airports
  - Cleveland Hopkins International Airport (CLE)
  - Miami International Airport (MIA)
  - John F. Kennedy International Airport (JFK)

  and three small, general aviation (GA) airports
  - Ohio University Airport (OU)
  - Burke Lakefront Airport (BL)
  - Tamiami Airport (TA)


MIA ATCT

Measurement Coordination (2)

- Access to airport movement area has become more complicated in the post September 11 era
  - Strict security procedures must be followed to gain access to the airport surface area—requires careful coordination with airport management
- Principle objective when planning a measurement activity is to minimize impact to airport operations

JFK ATCT

Measurement Coordination (3)

- Before any measurements, FAA Spectrum Office conducted an RFI study (clean)
- NASA obtained a Special Temporary Authorization to transmit at the test frequency from NTIA

Selected "cat walk" at ATCT sub-junction level for Tx

- Good field of view
- Access to AC power

Measurement Coordination (4)

- Prepared a measurement plan with desired
  - data recording locations
  - procedural approach
  - number of personnel involved
- Plan evaluated w/FAA for
  - accessibility
  - time of day
  - aircraft traffic activity
  - airport ingress/egress requirements
  - driving rules
- Final measurement plan evaluated & approved by FAA

Measurement Coordination (5)

- MIAMI aerial view, with numbered measurement locations

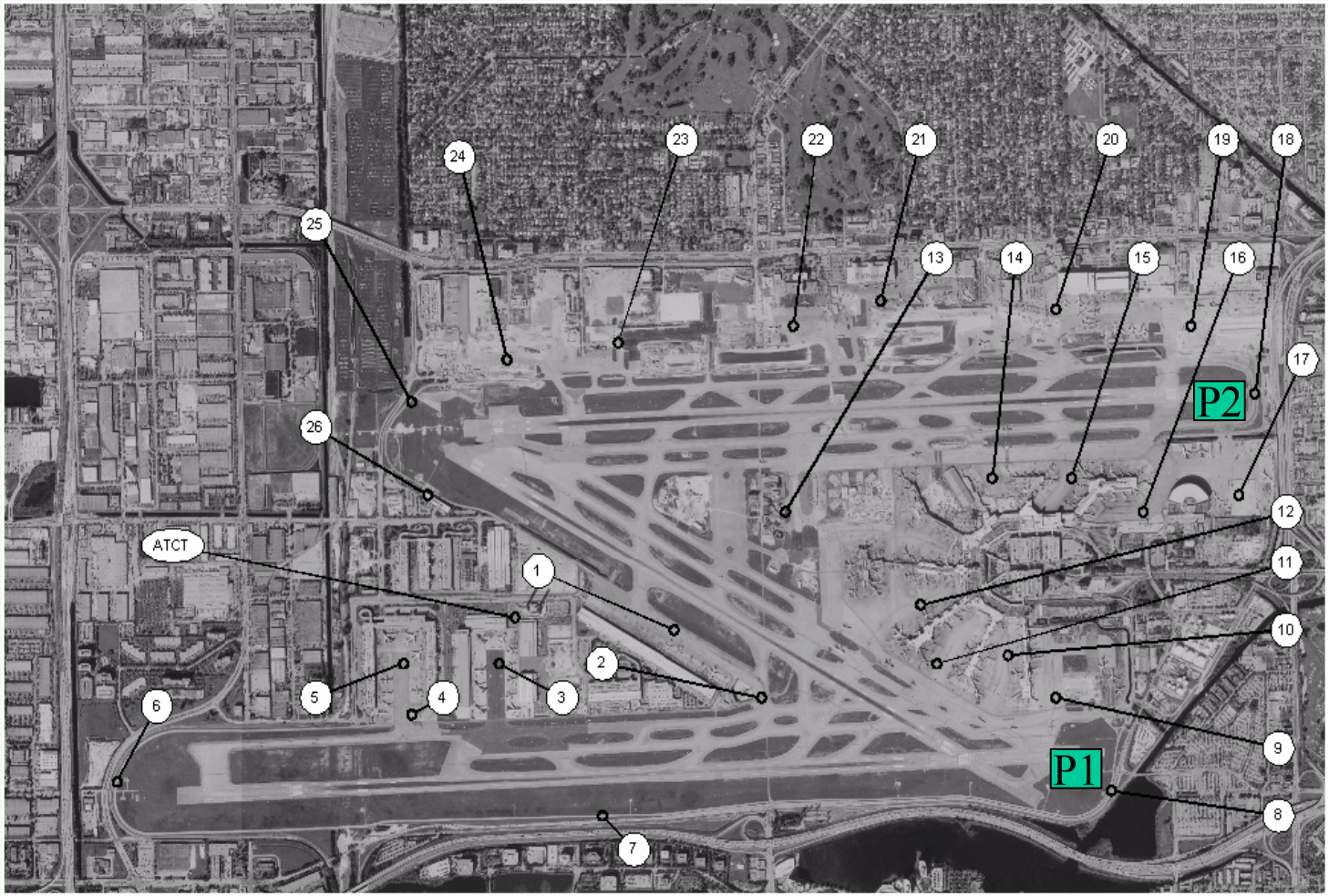

- Covered
  - –Taxiways
  - –Gates
  - –Cargo areas
  - –Access roads
- Both LOS and NLOS sites
- Also conducted mobile tests w/Tx at P2

- to #25, RMS-DS transitions
- (back to #34, field site meas)

Channel Characterization Overview

- Accurate, thorough channel characterization requires combination of 3 inter-related components:
  - *Analysis*: validate against theory, guide measurements
  - *Measurements*: data to build models, affirm theory, help classify, and identify unforeseen conditions
  - *Simulations*: create models for consistent evaluation of comparative system designs
- All results (analytical and measurement) we obtain are directly usable by engineers evaluating and/or designing communication systems for this application

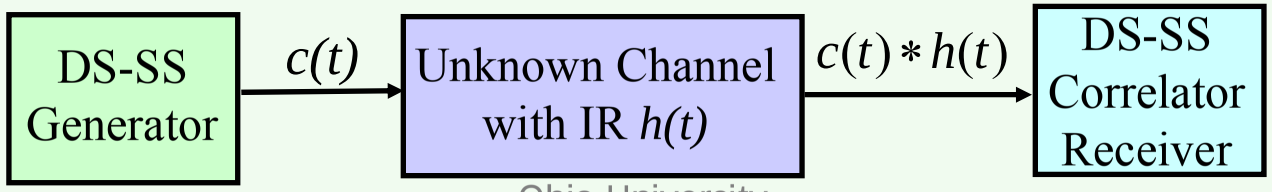

Channel Characterization Method

- Channel "sounding" is transmission and subsequent reception of a test signal, from which we can infer channel characteristics: the impulse response
- Common test signal is a spread spectrum (direct sequence) signal, whose known correlation properties can be exploited to estimate channel's impulse response

What is the channel?
A wireless channel is the complete (set of) transmission path(s) taken by an electromagnetic signal from transmitter to receiver, in the band of interest, over the spatial region of interest.

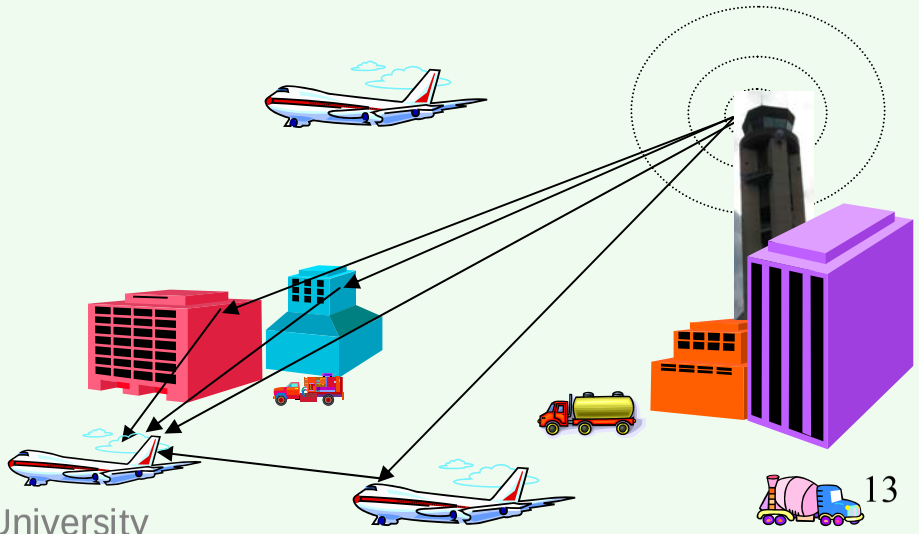

Channel Impulse Response (CIR)

$$h(\tau;t)=\sum_{k=0}^{N-1} z_k(t)\alpha_k(t)\exp\{j[\omega_{D,k}(t-\tau_k(t))-\omega_c(t)\tau_k(t)]\}\delta[t-\tau_k(t)]$$

- $h(\tau;t)$= response of channel at time t, to impulse input at time t-τ ; model as *random* and *time-varying*
- Path amplitudes $\{\alpha_k\}$ depend upon
  - Path loss, shadowing loss
  - Reflection, diffraction, absorption losses
  - Amplitudes/phases of components within $\Delta\tau$ *(20 ns)*
- $z_k(t)$ = "persistence" process ($\in\{0,1\}$) to account for finite "lifetime" of multipath components
- Doppler: $\omega_{D,k}=2\pi f_{D,k}$; $f_{D,k}<<f_c$ except for very high velocity platforms (e.g., LEO satellites)
  - $2\pi f_c\tau_k$ can change rapidly, since f_c large

Airport Surface Environment

- Airport movement area is a dynamic environment
  - airline ramp activities such as baggage handling, fueling, catering taking place throughout the day
  - aircraft also taxiing, pushing into, and pulling out of gates
  - airport security vehicles, other ground vehicles moving about

Airport Surface Environment (2)

- Airport surface area classification: 3 regions
  - **LOS-O**: Open areas, e.g., runways, some taxiways
  - **NLOS-S**: mostly NLOS w/dominant Specular component plus low energy multipath components, e.g., near terminals
  - **NLOS**: obstructed LOS, largest DS, e.g., near gates

- Aircraft & ground vehicles generally inhabit all three regions; over long-enough durations, channel is statistically non-stationary
- Large buildings present persistent, long-delay multipath, in contrast to most terrestrial models

Measurements: Example Photos

Mobile Measurements, MIA, June 2005

Measurements: Example Photos (2)

Point-to-Point Measurements, MIA, June 2005

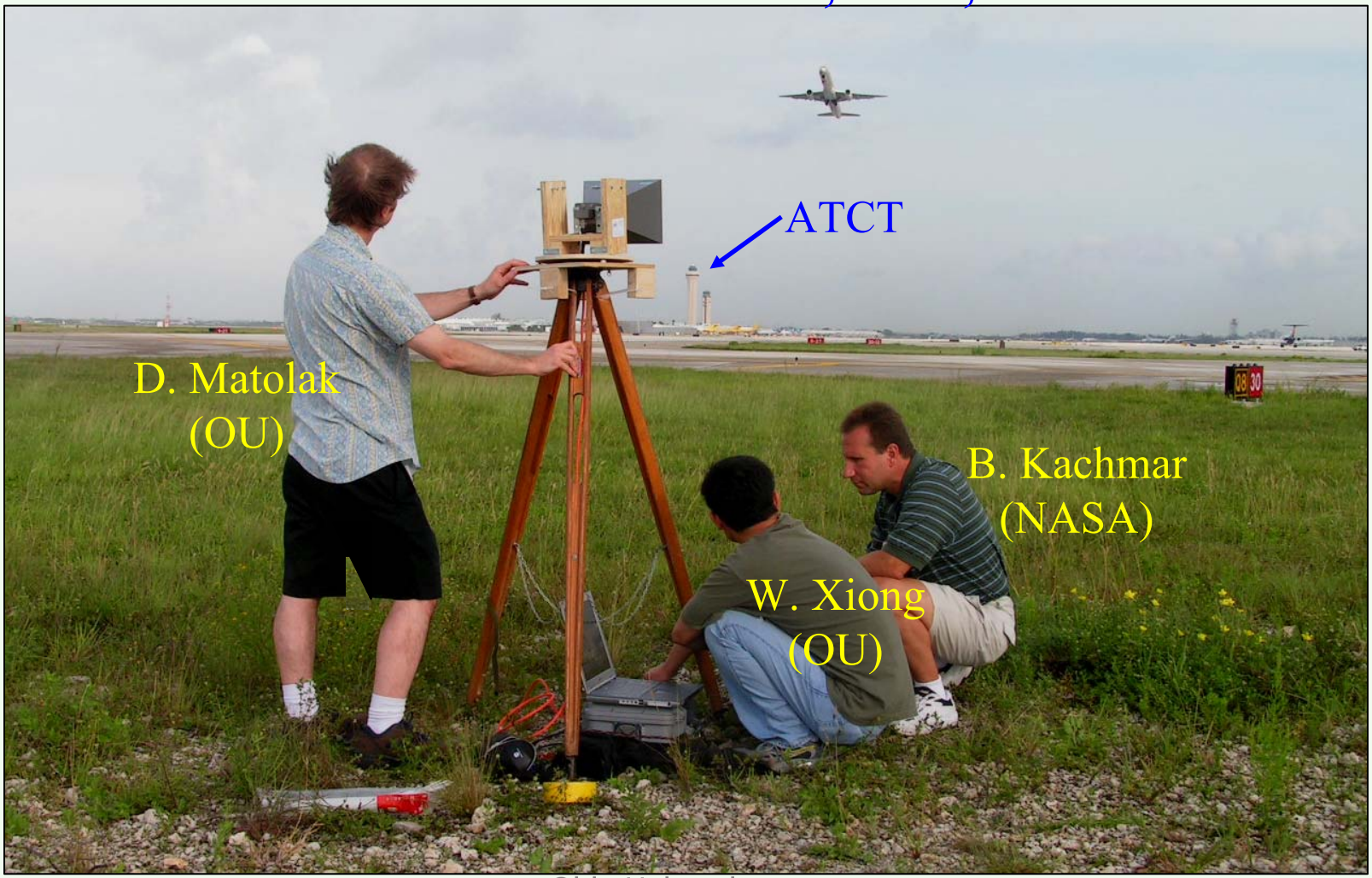

Measurements: Example Photos (3)

View from ATCT, JFK, August 2005

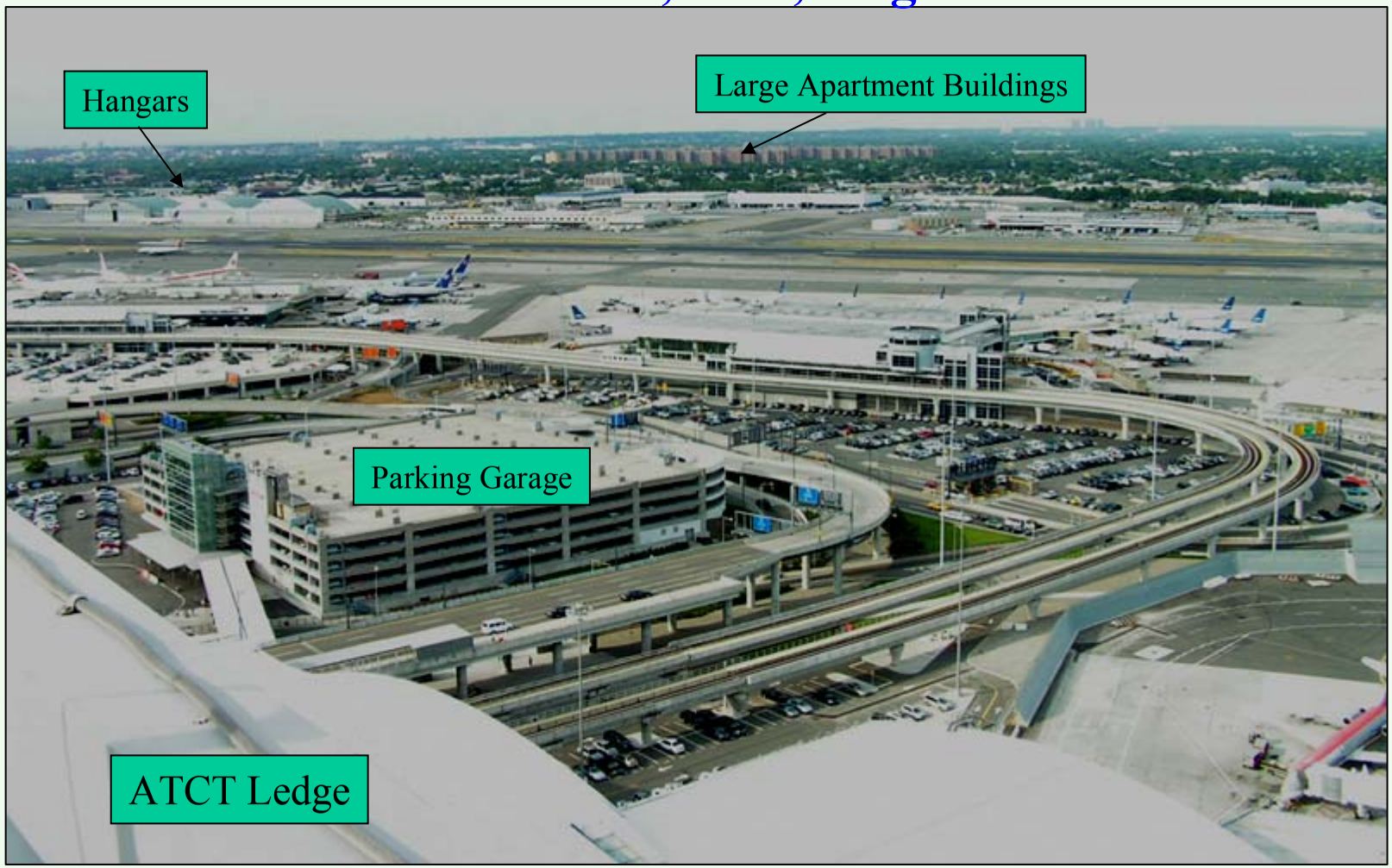

Channel Statistic Definitions

- **Delay Domain**
- RMS-DS: $\sigma_\tau = \sqrt{\dfrac{\sum_{k=0}^{L-1} \tau_k^2 \alpha_k^2}{\sum_{k=0}^{L-1} \alpha_k^2} - \mu_\tau^2}$
- Mean Energy Delay:

$$\mu_\tau = \frac{\sum_{k=0}^{L-1} \tau_k \alpha_k^2}{\sum_{k=0}^{L-1} \alpha_k^2}$$

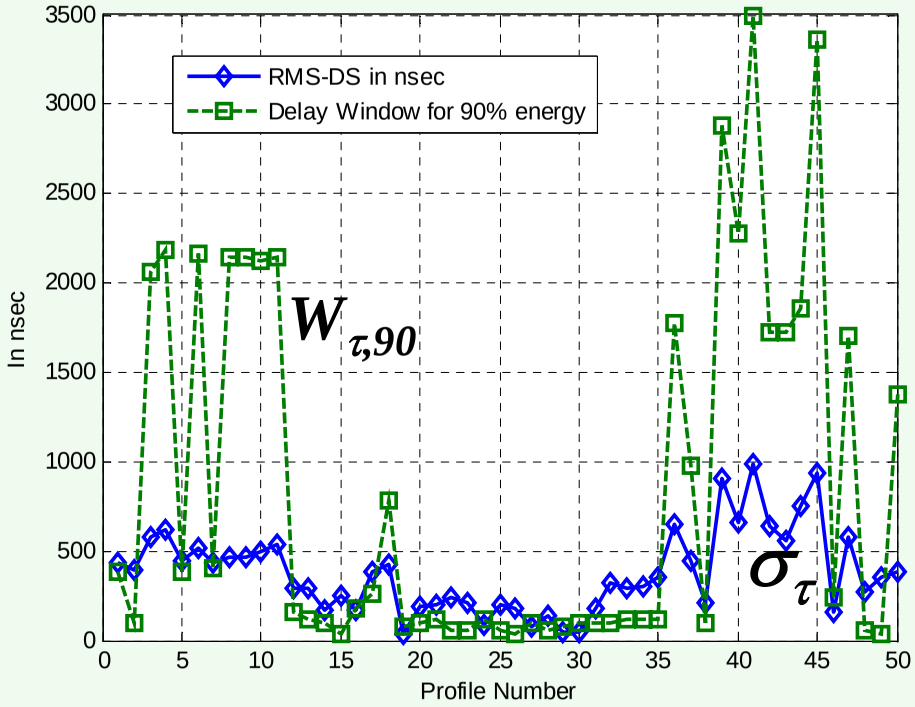

- Delay Window $W_{\tau,x}$ = the length of the middle portion of the CIR containing x% of the total energy of the CIR

Channel Statistic Definitions (2)

- **Frequency Domain**
- Correlation (~coherence) bandwidth, defined as extent in frequency for which channel affects signal equally
- FCE: time variations of complex amplitudes of different "spectral lines" directly crosscorrelated w/time variations of reference spectral line
  - Crosscorrelation=$\gamma_H(a_{ref},a_i)$, where a_i is amplitude of spectral line at freq. index i, and a_{ref} is amplitude at the ref. freq., i.e.,

$$a_{ref,j} = |H(f,t)|_{f=f_{ref},t=t_j}$$

$$\gamma_H(a_{ref},a_i) = \frac{1}{N}\sum_{j=1}^{N} a_{ref,j}a^*_{i,j}$$

$$FCE = \frac{\gamma_H(a_{ref},a_i)}{\sqrt{\gamma_H(a_{ref},a_{ref})\gamma_H(a_i,a_i)}};$$

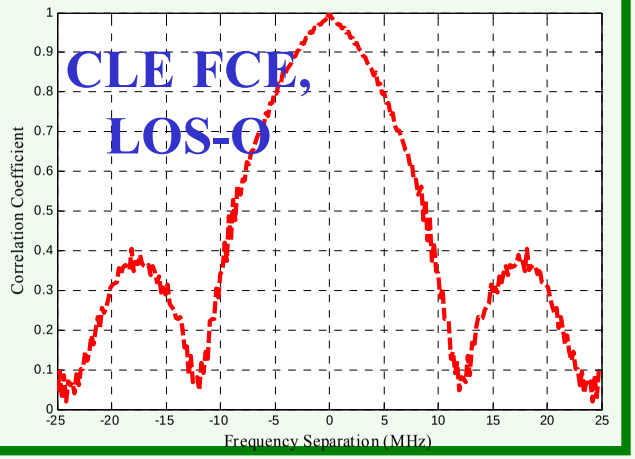

Mobile ATCT Measurements (1)

Measured RMS-DS [min; mean; max] (ns), Three Settings						
Airport	**Mobile**			**Point -Point**	**Field Site Transmit**	
	NLOS	**NLOS-S**	**LOS-O**	**LOS-O**	**NLOS**	**NLOS-S**
JFK	[800; 1,469; 2,456]	[21.4; 311; 798.7]	—	—	[802; 1,475; 2,433]	[5.8; 317.3; 799.5]
MIA	[1,000; 1,513; 2,415]	[23.1; 459; 999.9]	—	[5.6; 163; 249]	[1,000; 1,625; 2,451]	[8; 443; 997]
CLE	[500; **1,206**; 2,472]	[125; **295**; 499]	[14; **65**; 124]	[1; 18.12; 202]	—	— —
OU	—	[14; 293; 2,416]	—			
BL	—	[126; 429; 2,427]	[5; 44; 124]			
TA	[502; 1,390; 2,404]	[15; 256; 499]	—			

Over 51,000 total PDPs collected in 6 airports:

- ~ 35,000 for mobile setting
- ~ 5,000 for point-to-point setting
- ~ 11,800 for airport field site

Mobile ATCT Measurements (2)

- Power delay profiles—PDPs (received power vs. delay), after noise thresholding, for 50 MHz bandwidth

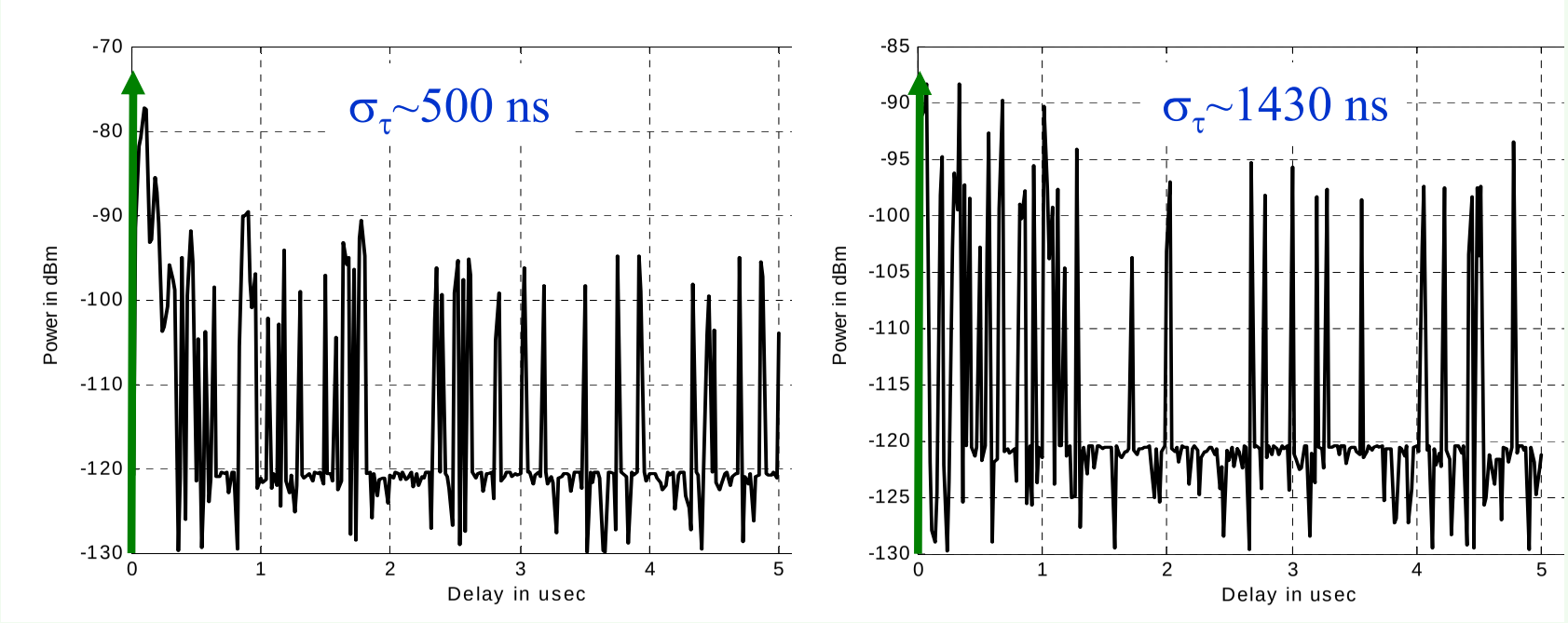

CLE, NLOS-S case

Significant multipath (~ 9 dB) up to $3T_c$ (0.06 μsec) + numerous weaker components

MIA, NLOS case

Significant multipath (~ 0 dB) up to $15T_c$ (0.3 μsec)

Mobile ATCT Measurements (3)

- MIA PDP: power vs. delay and vs. time, NLOS

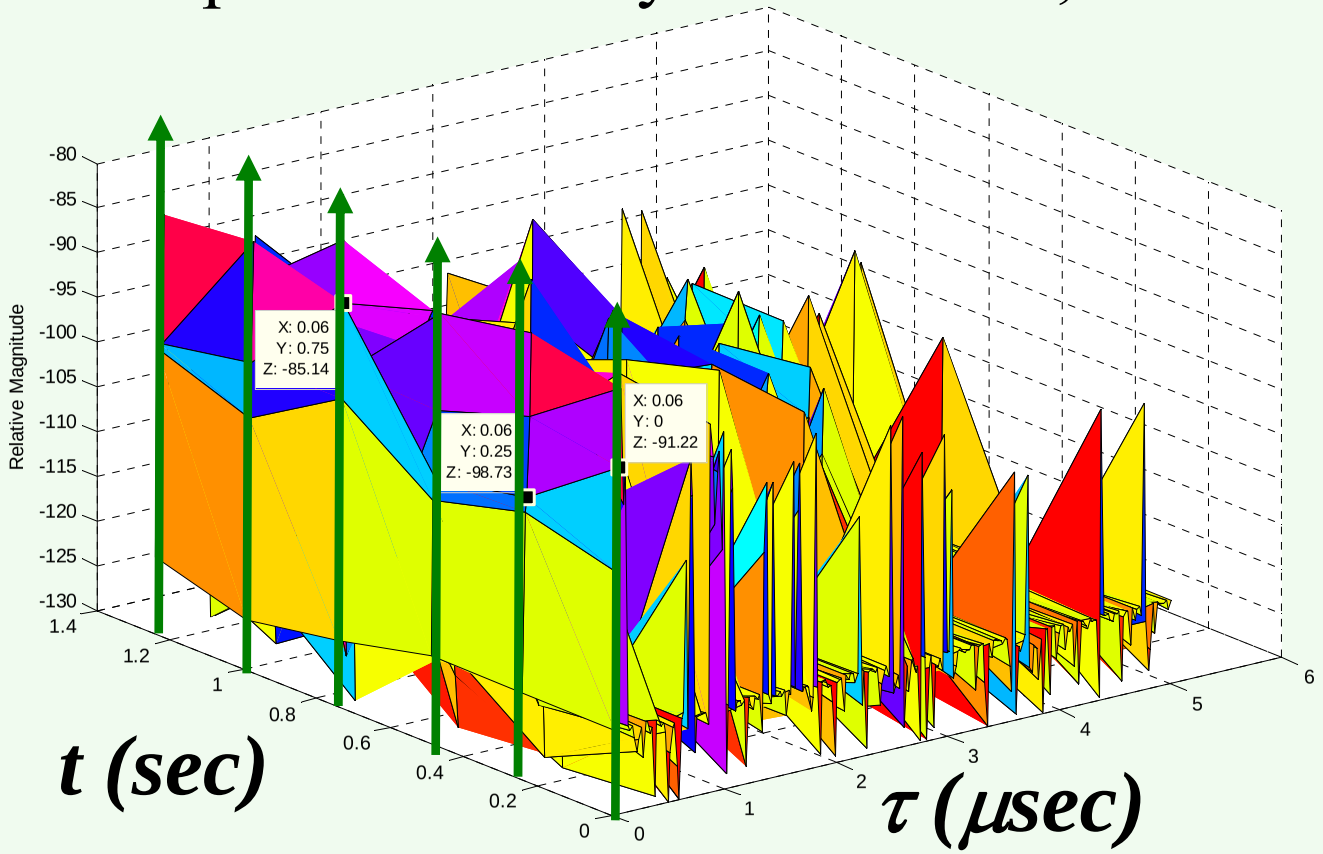

Fades of approximately 14 dB on main tap

Mobile ATCT Measurements (4)

- Plots of RMS-DS vs. profile index (time)

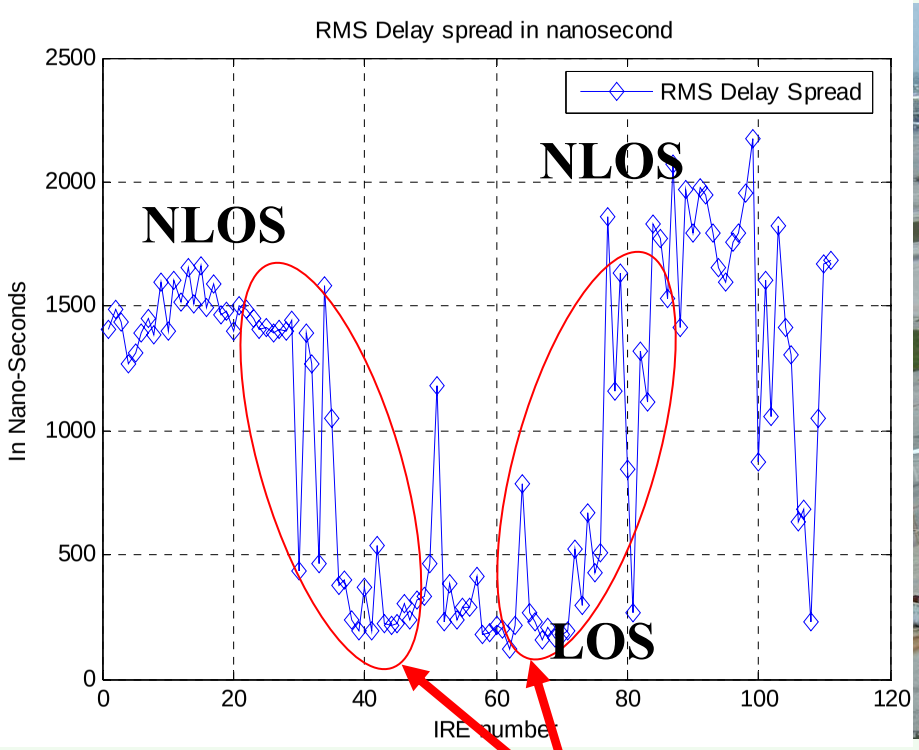

MIA: Multiple transitions to/from NLOS/LOS/NLOS

Mobile ATCT Measurements (5)

- Tap probability of occurrence (fraction of time), 50 MHz BW
- Threshold = 25 dB from main tap

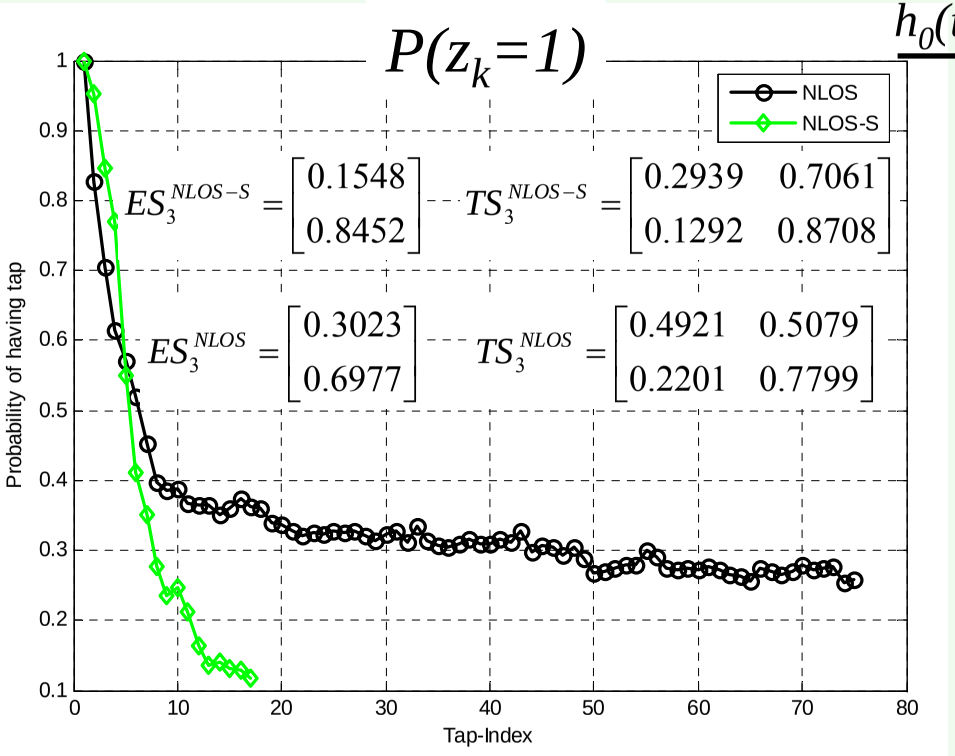

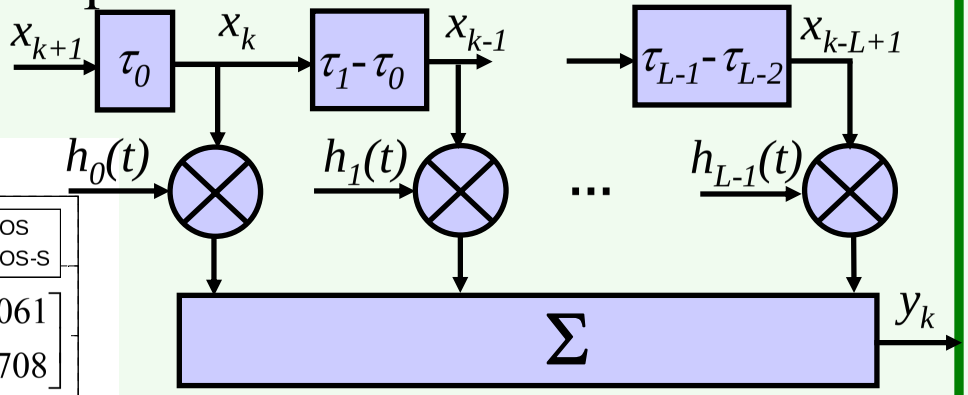

- NLOS-S: # taps L=18
- NLOS: # taps L=**75**

$$h_k(t) = z_k(t)\alpha_k(t)e^{j\phi_k(t)}$$

Mobile ATCT Measurements (6)

- Cumulative energy versus tap index for 50 MHz BW

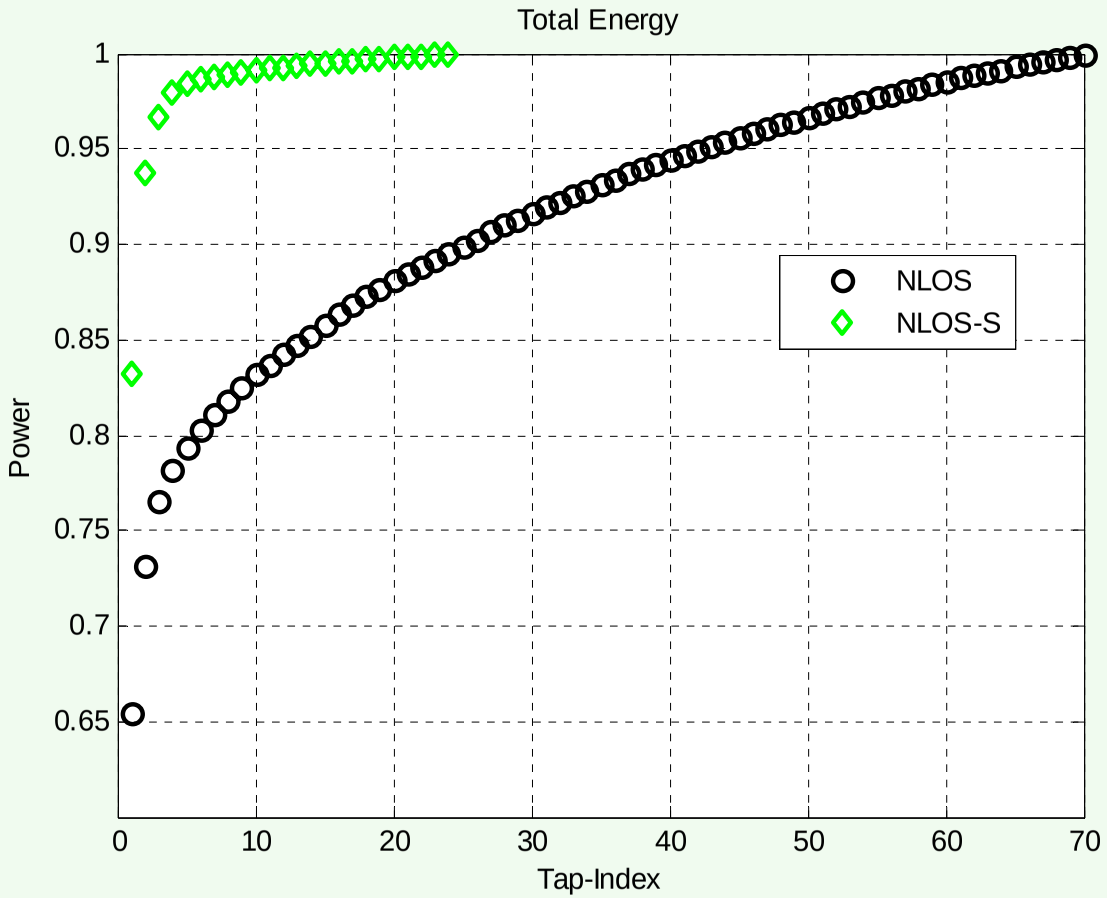

Tap Index	% Energy
NLOS-S	
4	98
9	**99**
NLOS	
10	83
15	85.8
20	88.1
25	90
30	91.6
35	93.2
40	**94.5**

Mobile ATCT Measurements (7)

- Amplitude distribution, MIA, NLOS

Tap #1

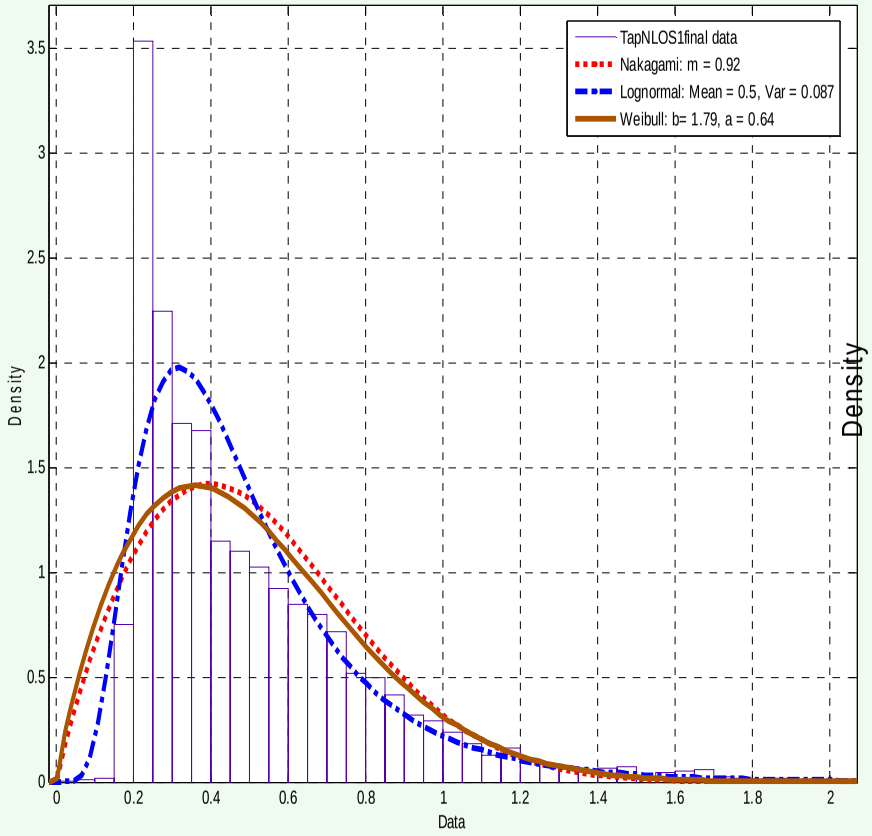

Tap #2

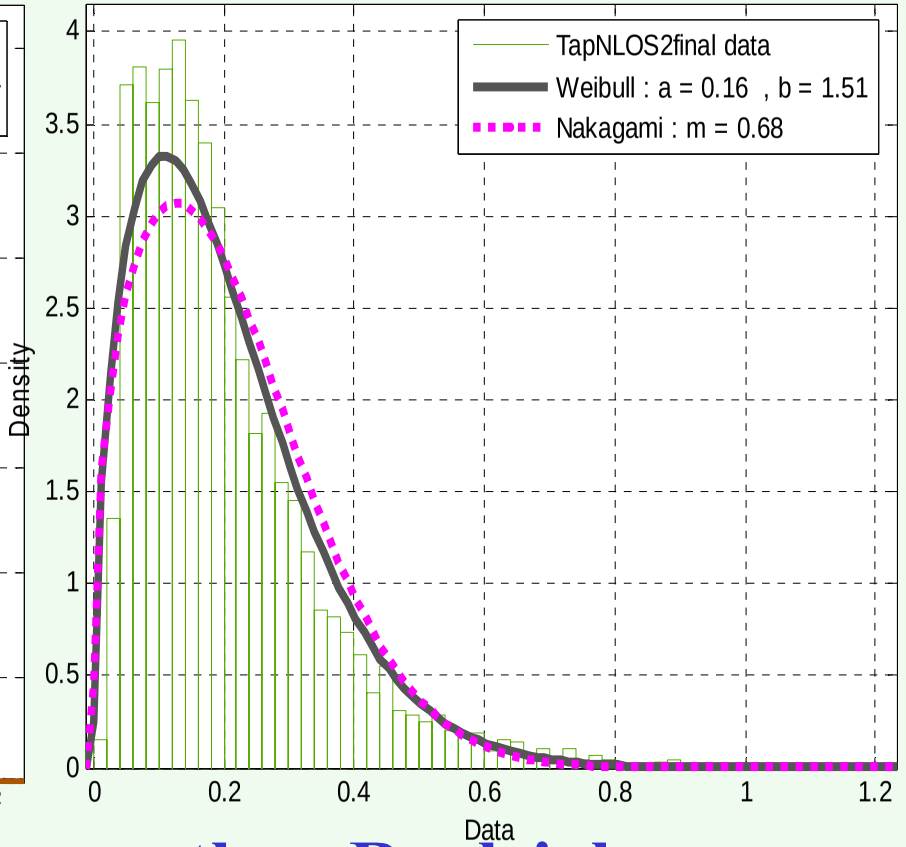

- **Both NLOS taps 1 & 2 worse than Rayleigh**

Mobile ATCT Measurements (8)

- Amplitude statistics for NLOS-S, 50 MHz bandwidth

Tap Index	Fractional Energy	Shape Parameter (*b*)	Alternate Distribution Parameter
1	0.7666	3.81	K = 6.8 dB
2	0.1042	1.66	**m = 0.78**
3	0.0310	1.86	m=0.98
4	0.0167	1.91	m=1.09
5	0.0084	1.97	m=1.16
6	0.0069	1.86	m=1.04
7	0.0049	2.04	m=1.21
8	0.0045	1.89	m=1.01
9	0.0043	1.90	m=1.05

- Weibull probability density
  - $f_w(x) = \frac{b}{a^b} x^{b-1} e^{-\left(\frac{x}{a}\right)^b}$
  - b = shape factor, determines fading severity
  - a = scale parameter

$$= \sqrt{\frac{E(x^2)}{\Gamma\left(\frac{2}{b}+1\right)}}$$

Mobile ATCT Measurements (9)

- Time series of Taps 1 and 2, NLOS-S, 50 MHz BW

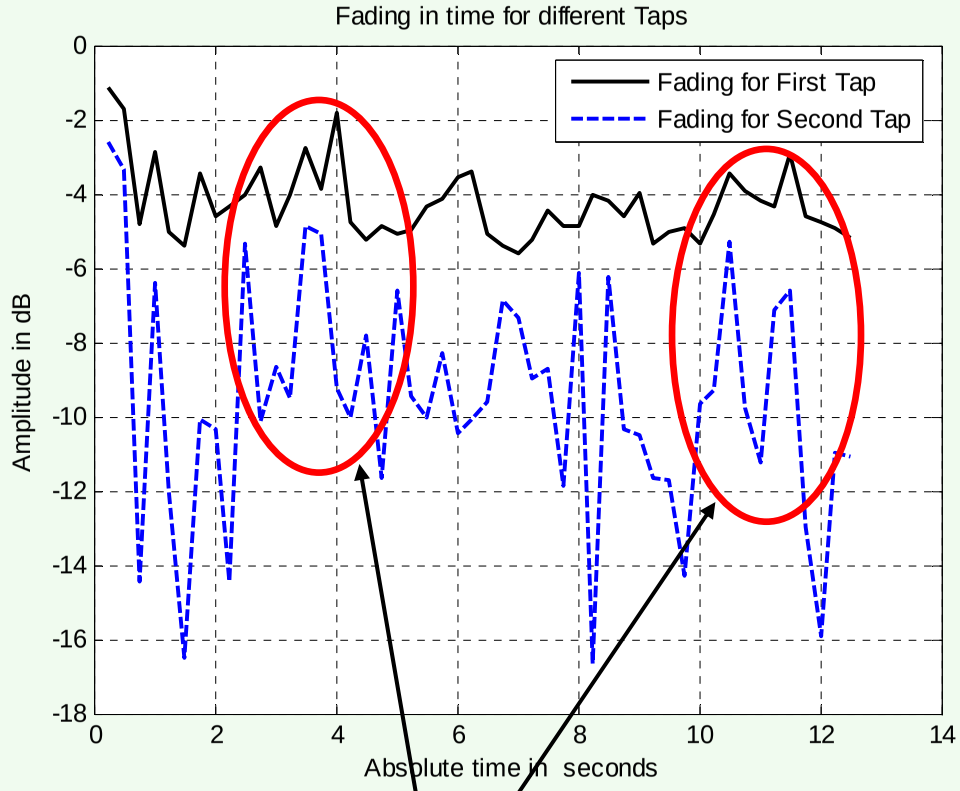

Highly correlated taps

- Tap correlations for NLOS-S, 50 MHz BW

Taps	(Min, Max)
(1,2)	(-0.33,**0.706**)
(1,3)	(-0.34,**0.43**)
(1,4)	(-0.39,0.31)
(1,5)	(-0.38,**0.74**)
(1,6)	(-0.42,0.13)
(1,7)	(-0.42,0.11)
(1,8)	(-0.38,0.0078)
(1,9)	(-0.43,0.18)

Mobile Field Site Measurements (1)

- Airport Field Sites useful in network to
  - Provide adequate signal strength in areas shadowed and distant from ATCT
  - Reduce channel dispersion
- Video clip of measurement in MIA
- Points 13-17, Tx at “P2” site
- (to aerial photo)
- Video Clip 0038
- PDP Animation

Tamiami, Kendall, FL

Mobile Field Site Measurements (2)

- Distribution of RMS-DS for Field Site and ATCT Tx

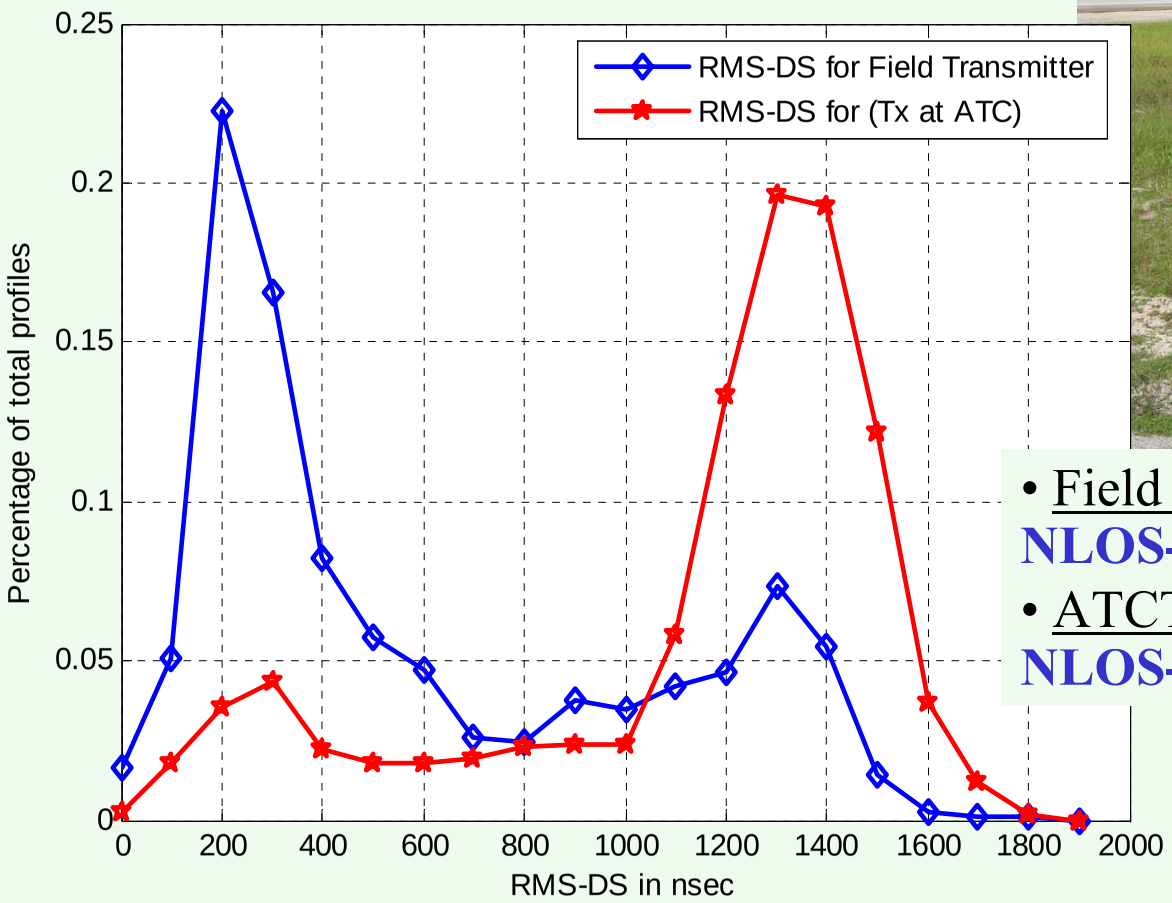

- Field Site Tx: **75% profiles in NLOS-S and 25% in NLOS**
- ATCT Tx: **23% profiles in NLOS-S and 77% in NLOS**

Channel Model Construction

- 3-state Markov chain to model transitions between propagation regions
- 2-state Markov chain for tap persistence processes
- Correlated Weibull amplitude fading

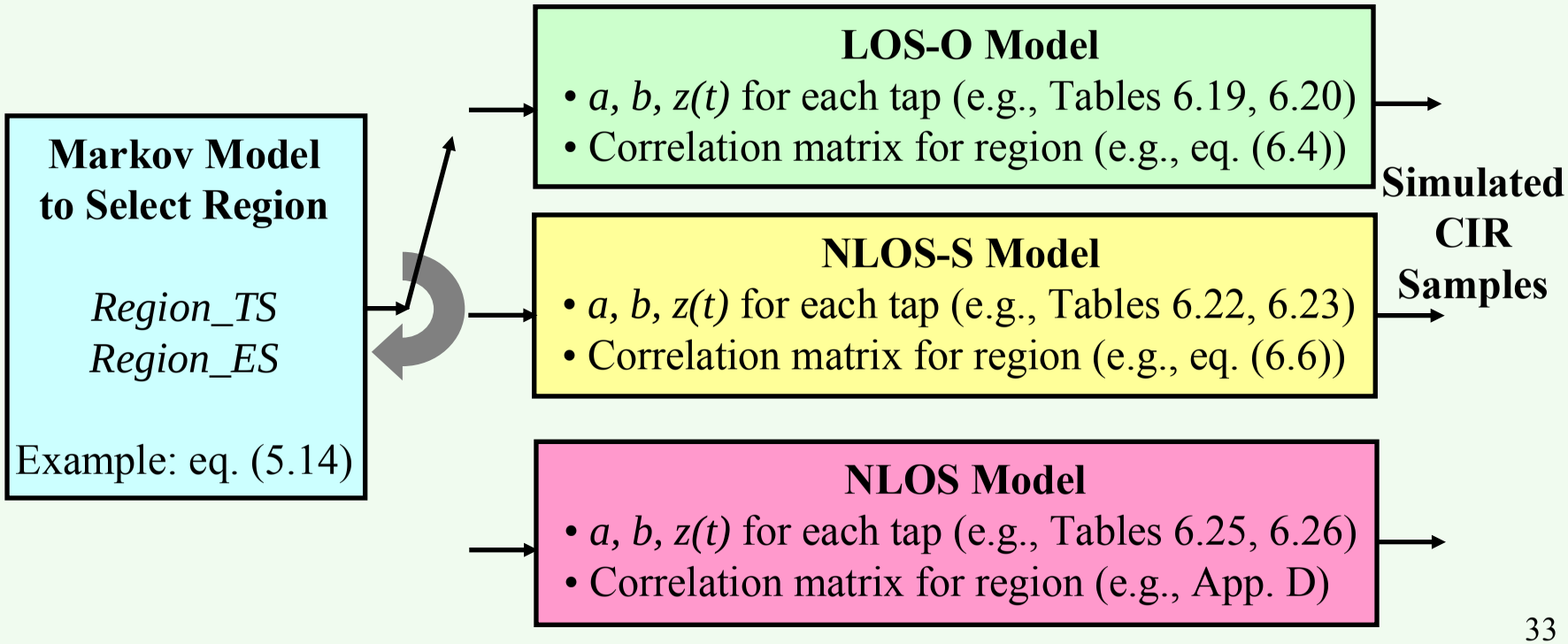

Channel Model Construction (2)

- Select channel BW (20 MHz), airport size (Lg)
- Using mean RMS-DS, # NLOS taps is 32
  - Reduce to ***L*=25**, account for 95% energy
- Select tap correlation matrix (worst-case, avg.,...)
- Obtain tap amplitude statistics →
- Obtain tap persistence process parameters ↓

Tap Amplitude Statistics

Tap Index	Weibull Factor (*b*)	Tap Energy
1	1.98	0.4953
2	1.5	0.0587
3	1.6	0.0261
4	1.6	0.0223
5	1.6	0.0191
6	1.55	0.0193
7	1.66	0.0174
8	1.65	0.0164
9	1.67	0.0155
10	1.65	0.0159
11	1.56	0.0168
12	1.59	0.0164
13	1.61	0.0154
14	1.61	0.0151
...	...	...

Tap Persistence Process Parameters

Tap Index	Probability State 1	Probability State 0	P_{00}	P_{01}	P_{10}	P_{11}
1	1.0000	0	*n/a*	*n/a*	0	1.0000
2	0.8540	0.1460	0.2409	0.7591	0.1298	0.8702
3	0.7168	0.2832	0.3772	0.6228	0.2462	0.7538
4	0.6563	0.3437	0.4535	0.5465	0.2863	0.7137
5	0.6321	0.3679	0.4875	0.5125	0.2981	0.7019
6	0.6065	0.3935	0.5119	0.4881	0.3168	0.6832
...	...	...	...	...	...	...

Channel Model Construction (3)

- Example persistence process and propagation region Markov chain outputs

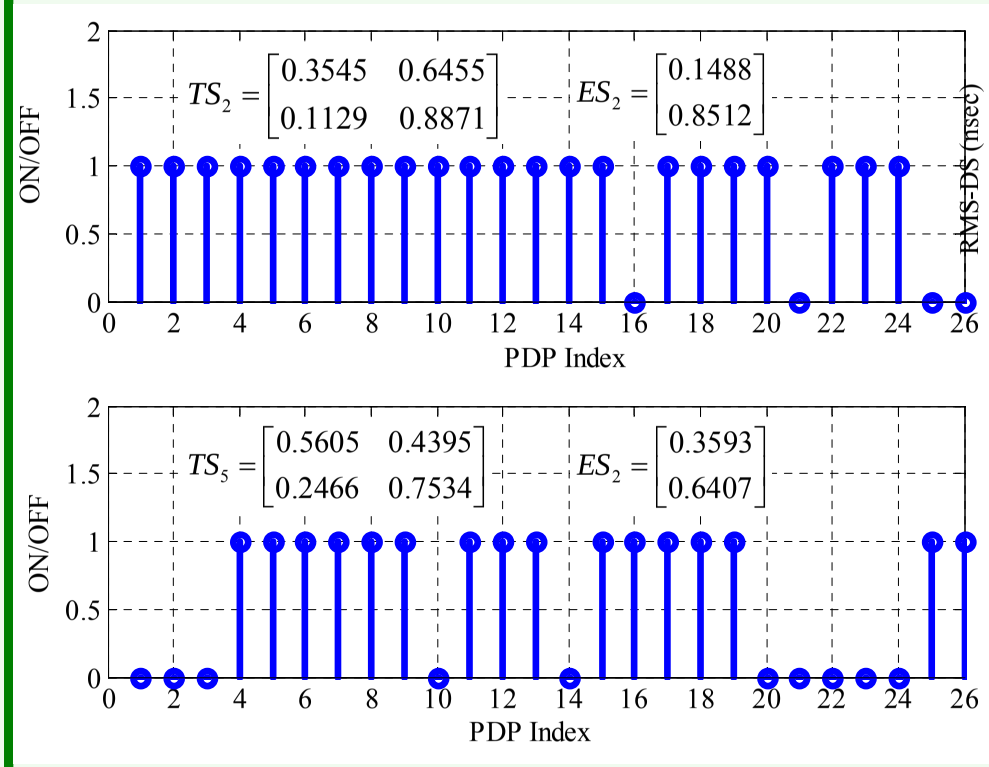

Tap Persistence, Taps 2, 5

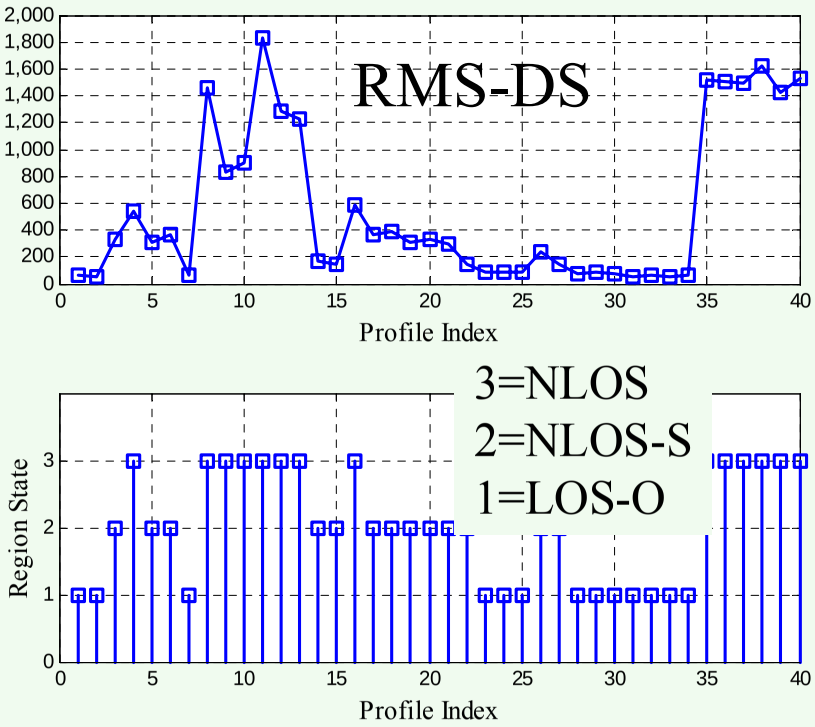

Propagation Region

Channel Model Construction (4)

- Example tap fading amplitudes, Large Airport, NLOS-S

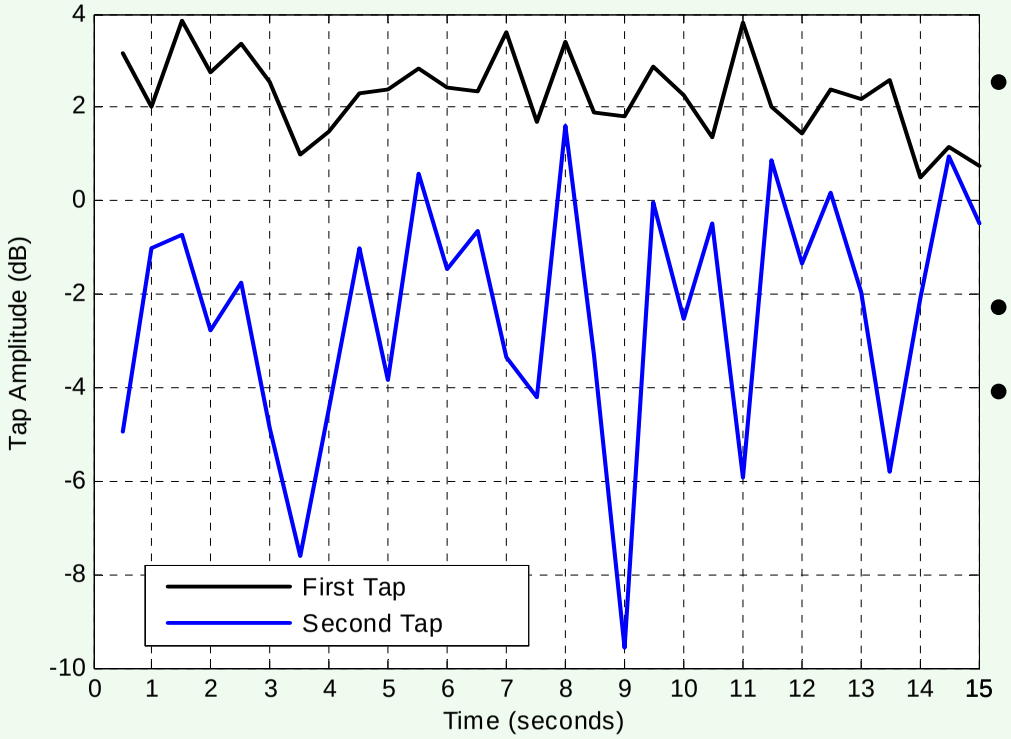

- Weibull Fading Parameters
  - Tap 1: $E(\alpha^2)$=0.79, b=4.8
  - Tap 2: $E(\alpha^2)$=0.1 , b=1.7
- $r_{12} = 0.79$
- Developed algorithm to generate multivariate, correlated Weibulls with arbitrary $E(\alpha^2)$, b

Channel Model Evaluation

- Model comparison: SF & HF vs. Measured Data

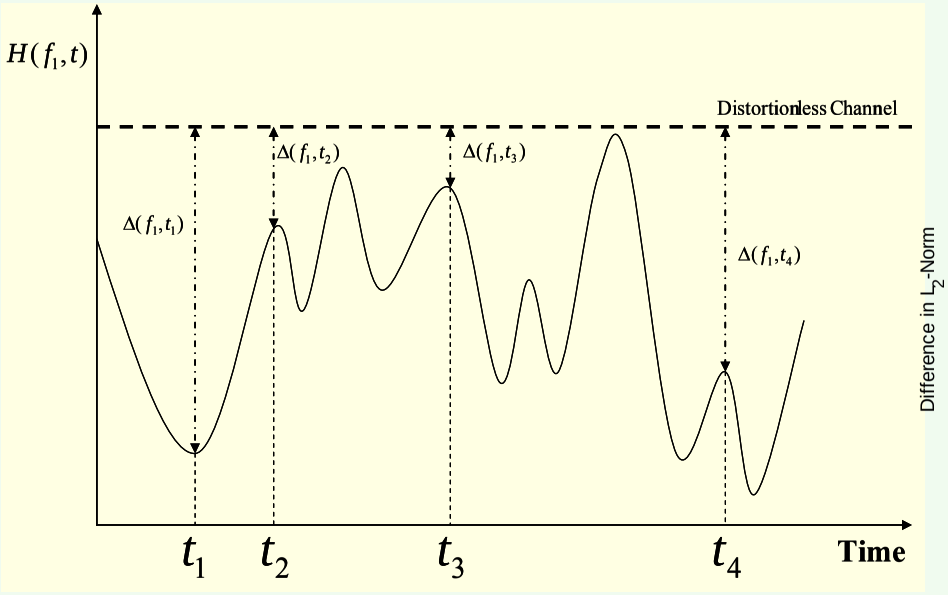

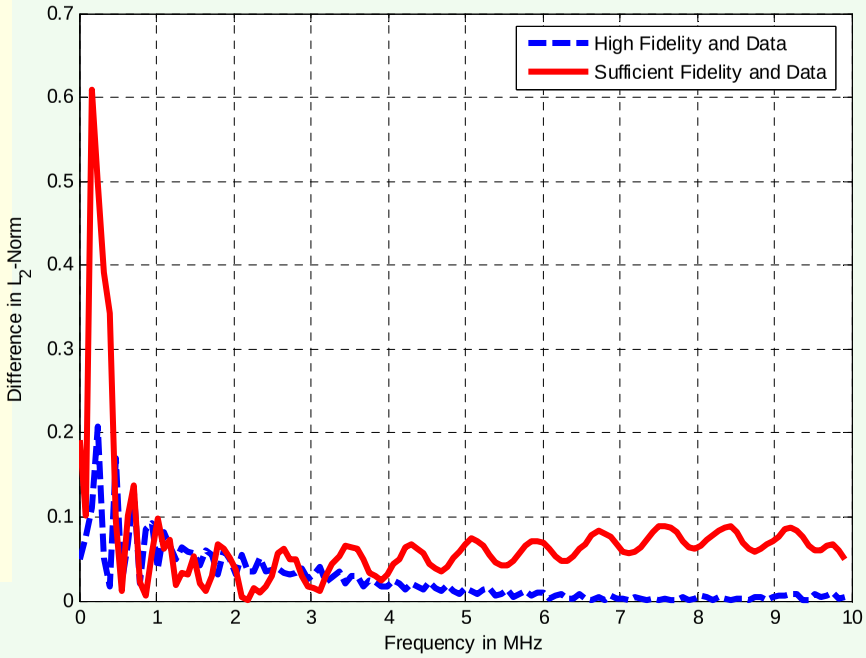

$$\Delta_M(f,t) = 1 - H_M(f,t)$$

$$L_2 - norm_{(t)} = \left\| \Delta_M(f_j,t) \right\|_2 = \sqrt{\int_{\{t\}} \Delta_M^2(f_j,t)\,dt} \cong \sqrt{\sum_{i=1}^{N_M} \Delta_M^2(f_j,t_i)}$$

Summary (1)

National Aeronautics and Space Administration

Federal Aviation Administration

- Provided motivation to characterize the 5 GHz MLS extension band channel around airport surface areas
  - Need for effort from the point of view of efficient communication link design, and band protection

- Recent measurement campaign multiple airports described, including
  - Coordination w/local authorities required for successful tests
  - Description of equipment, measurement process
  - Example measured results
  - Example modeling results

Summary (2)

- Correlated scattering in all regions of airport
- Amplitude statistics for some taps worse than Rayleigh
- Statistical non-stationarity
- Both high-fidelity and sufficient fidelity channel models developed

$$\mathbf{R}_{\alpha}^{\mathrm{NLOS-S}} = \begin{bmatrix} 1 & 0.7881 & 0.2940 & 0.3485 & 0.4782 & 0.4581 & 0.8969 & 0.5644 \\ 0.7881 & 1 & 0.3134 & 0.6588 & 0.4255 & 0.8239 & 0.7768 & 0.6160 \\ 0.2940 & 0.3134 & 1 & 0.5758 & 0.8606 & 0.6958 & 0.4222 & 0.9695 \\ 0.3485 & 0.6588 & 0.5758 & 1 & 0.6939 & 0.6605 & 0.9513 & 0.7965 \\ 0.4782 & 0.4255 & 0.8606 & 0.6939 & 1 & 0.9181 & 0.4653 & 0.8869 \\ 0.4581 & 0.8239 & 0.6958 & 0.6605 & 0.9181 & 1 & 0.6528 & 0.6052 \\ 0.8969 & 0.7768 & 0.4222 & 0.9513 & 0.4653 & 0.6528 & 1 & 0.7502 \\ 0.5644 & 0.6160 & 0.9695 & 0.7965 & 0.8869 & 0.6052 & 0.7502 & 1 \end{bmatrix}$$

Field Site Measurement Summary

- Can reach areas that are “hard-to-reach” from ATCT Tx
- Comparatively, channel is less dispersive than ATCT Tx mobile channel
- A very high-fidelity channel model can be implemented with lower complexity than for the ATCT mobile measurement model

Future Work

1. Refine channel models for VTV applications

- *<u>Goal</u>: Develop high-fidelity, non-WSSUS models for Vehicle-to-Vehicle channels, for Intelligent Transportation Systems (ITS)*

2. Wideband air-ground channel characterization in 960-1024 MHz aeronautical spectrum, for future air-ground communications

- *<u>Goal</u>: Develop wideband statistical channel models applicable to the 960-1024 MHz aeronautical (DME) band*

3. Evaluation of candidate communication system (IEEE 802.16, cellular) performance on airport surface in MLS extension band

- *<u>Goal</u>: Determine expected performance of best technology candidate(s) for airport surface communications deployment*

Questions??